

Tribocorrosion and metal release from austenitic stainless steels 304 and 201 in simulated cassava food contact

R. Addai^{a,1}, T.E. Olowoyo^{a,1}, J.D. Henderson^b, T.E. Standish^b, U. Eduok^a, Y.S. Hedberg^{a,b,*}

^a Department of Chemistry, The University of Western Ontario, London, Ontario N6A 5B7, Canada

^b Surface Science Western, The University of Western Ontario, London, Ontario N6G 0J3, Canada

ARTICLE INFO

Keywords:

Chromium
Nickel
Manganese
Friction

ABSTRACT

Cassava is the third most significant calorie source in the tropics. Its processing has changed from traditional methods to stainless steel processing machines. This study investigated the influence of cassava on metal release from two common stainless steels, ASTM 304 and 201, with and without friction, and on tribocorrosion (multi-analytically) of 304. Cassava was relatively corrosive and hindered repassivation of the surface oxide of stainless steel, but it also acted as a lubricant against mechanical friction. The combined action of friction and cassava caused a significant increase in iron, chromium, nickel, and manganese release from the stainless steels (30–35-fold increase compared to no friction, and 4–12-fold increase compared to water without cassava but with friction).

1. Introduction

Cassava (*Manihot esculenta* Crantz), also known as manioc, tapioca, or yuca, belongs to the family Euphorbiaceae and is a perennial woody shrub distinguished by its tuberous roots [1]. Originating from South America, cassava is now extensively grown in tropical and subtropical areas across Asia, Africa, and Latin America. It holds the distinction of being the third most significant calorie source in the tropics, following rice and maize [2]. In 2020, global cassava production was estimated at 303 million tonnes, and the leading producer was Nigeria, contributing 20% to the global output. Other substantial growers were the Democratic Republic of the Congo and Thailand [3].

Cassava roots are rich in energy and packed with various vitamins, minerals, and dietary fiber. The presence of cyanide in cassava roots poses a problem, but it is reduced during processing [4]. In Africa, over 80 % of cassava production serves as a crucial calorie source for human food, with more than half of it being utilized in various processed forms. In the Americas, approximately 40 % of cassava production is allocated for human consumption, while 30 % is directed toward livestock feed. In contrast, Asia operates as a net exporter of cassava products [5]. The primary constituent of cassava root is starch, which can make up to 80 % of the root's dried weight [6]. Cassava root can be processed into different products such as garri, cassava flour, cassava chips, and cassava starch.

Cassava flour is obtained by milling the dried raw cassava root [7]. After being harvested, the cassava root must be promptly consumed or transformed into more stable product forms such as flour. Any fresh roots should undergo processing within 2 to 3 days of being harvested [8]. The primary limitation faced in cassava processing is the swift decay of its roots. Once harvested, cassava roots possess a shelf-life of merely 24 to 48 h [9]. Cassava can be processed through traditional methods or processing machines. Cassava processing through traditional methods proves to be arduous, inefficient, time-consuming, and ineffective overall. The challenges emerge particularly during the grating and draining of the starchy fluid from the cassava dough, as conventional techniques demand extensive labor and consume significant amounts of time [8]. Cassava processing machines have stepped up to meet the increasing urban food demands for greater convenience, such as cassava flour-based bread [10]. Mechanization is essential for optimizing production, harvesting, and processing, leading to cost reduction and minimizing waste [8]. The processing machinery for cassava includes cassava harvesters, cassava graters, cassava pressing machines, mills, sifters, and fryers [8].

Stainless steels are usually used in making cassava processing machines and cookware utilized in preparing food such as fufu, which is a meal made from cassava flour commonly consumed in West African and Caribbean countries [11,12]. Material degradation of these stainless

* Correspondence to: Dept. Chemistry, Western University, N6A 5B7 Canada.

E-mail address: yhedberg@uwo.ca (Y.S. Hedberg).

¹ these authors contributed equally

steel processing machines can occur due to the combined effect of friction/wear and continuous processing of cassava, which can be corrosive. The material deterioration resulting from the simultaneous action of wear and corrosion is known as tribocorrosion [13]. Tribocorrosion can lead to the degradation and malfunction of cassava processing units, hence understanding the tribocorrosion mechanism and behaviors of stainless steel in the cassava processing environment has become important. In addition, metal release from stainless steel during processing or cooking could potentially have adverse health effects [14]. Therefore, it is important to conduct an accurate assessment in order to determine the extent of metal release and prevailing processes [15], as ingestion of harmful metals through food is one of the pathways of exposure for the general population throughout their lifetime [16].

Stainless steel ASTM grades 304 and 201 are frequently used in applications involving food due to their high corrosion resistance and good mechanical characteristics [14]. Stainless steel 304 and 201 are austenitic stainless steels containing a significant amount of chromium (Cr), and sufficient nickel (Ni) or manganese (Mn) to stabilize the austenite microstructure that gives these steels formability and ductility. 304 grade contains 18 % Cr and 8 % Ni and is mostly used in household appliances and the food industry. Grade 201 stainless steel was created in response to soaring Ni prices. As one of the cheaper options, grade 201 is very appealing to the food industry, especially in developing countries. An austenitic 201 contains 16–18 % Cr and 3.5–5.5 % Ni. It contains higher amounts of Mn (5.5–7.5 %) and nitrogen (N), and lower amounts of Ni than 304 steel [17].

Minerals such as Cr, iron (Fe), and Mn play crucial roles in the proper functioning of the human body. However, excessive levels of these metals in the body can give rise to health issues. Dietary Cr is primarily found in the form of Cr(III), and a significant portion of the Cr content in food comes from the utilization of stainless steel food processors and containers during food processing [18]. Its advised daily intake (trivalent Cr) is a maximum of 250 µg/day [19]. Fe is found in most foods and beverages. The average daily dietary intake of Fe in the European Union (EU) ranges from 10–22 mg/person/day [20]. There have been a few cases where significant amounts of Fe were released from materials that come in contact with food, for example the release of 2500 mg/kg Fe from a wok and a cast iron skillet [21]. Although Mn is necessary for health, inhalation or ingestion of high levels can lead to unfavorable health outcomes [22]. According to a report [23], the average daily intake of Mn is estimated to be around 2.16 mg/person/day in adults. Ni is present in small quantities in various food items (0.001–0.01 mg/kg) [24]. Allergic reactions to Ni are caused by the absorption of Ni through the skin. Patients suffering from allergic contact dermatitis to Ni might experience a worsening of their eczema symptoms through oral intake of even minimal quantities of Ni. This can occur through the consumption of Ni-rich food items or the ingestion of foods and beverages contaminated by Ni-containing materials [25,26]. The World Health Organization [27] established a tolerable daily intake threshold for Ni, 0.012 mg/kg of body weight/day (equivalent to ~0.7 mg/day), based on human data.

This study investigates the influence of cassava flour (slurry) on Cr, Fe, Mn, and Ni release from two common food contact stainless steels, 304 and 201, during stirring (with friction) and static conditions and the tribocorrosion of stainless steel 304 in the presence and absence of cassava. The study attempts to determine the physical and chemical extent of degradation, and the synergistic effects (tribocorrosion) that cassava has on these common food contact stainless steels.

2. Materials and methods

2.1. Sample preparation

Austenitic American Society for Testing and Materials (ASTM) 304 and ASTM 201 stainless steel sheets (1 mm thick) were obtained from the International Stainless Steel Forum, Brussels, Belgium. Their

nominal bulk alloy composition is given in Table 1. The 304 and 201 stainless steel sheets were cut into square pieces of 15 mm by 15 mm for stirring and static conditions, while 304 stainless steel sheets only were cut into square pieces of 18 mm by 18 mm for tribocorrosion testing. The coupons were polished using a series of silicon carbide grinding papers down to P4000 grade to achieve the same surface condition for all samples. Then, the coupons were ultrasonically cleaned in acetone and ethanol (5 min each) and dried with nitrogen gas at room temperature before tribocorrosion testing. For stirring and static conditions, the samples were aged in a desiccator (relative humidity <10 %) at room temperature for 24 ± 1 h. This preparation procedure enables reproducible surface oxide growth and comparison with other studies [17].

2.2. Solution preparation

Solutions were prepared with cassava flour from Steda Tropical Foods Ltd (London, ON, Canada) and American Chemical Society reagent grade sodium chloride (NaCl) using Type I (ultrapure) water (18.2 MΩ-cm resistivity) from a Millipore Milli-Q Reference system. According to the package, the cassava flour powder contained cassava, granular potato, and plantain, with a total fat content of 0.4 g, carbohydrate 81 g, protein 5 g, fibre 0.9 g, and ash 3 g (per total of 100 g dry weight). For metal release tests under stirring (with friction) and static (no friction) conditions, a cassava slurry solution of 80 g/L cassava (without NaCl) and a natural pH of 5.6 was prepared. This cassava concentration was chosen because cassava slurry needs to be as highly concentrated as possible to mimic the stainless steel processing machines, which only contain the water in the cassava root. In a previous study by some of the authors of this study [15], 80 g/L whey protein solution was chosen based on actual protein drink concentrations, and that concentration was found as an upper limit for immersion and corrosion tests, including necessary digestion for metal release estimations.

To understand the contribution of cassava flour to metal release (from both stainless steel 304 and 201), reference solutions of only ultrapure water (not buffered) were prepared in parallel with the cassava slurry for both stirring and static conditions. Triplicate coupons were exposed to the two solutions (cassava slurry and reference) for each test condition (stirring and static for 0.5, 24, or 168 h) at room temperature. For stirring conditions, the coupons were exposed to 5 mL of the two solutions. For static conditions, the coupons were exposed to 8 mL of the two solutions. One blank sample (test solution only, without any coupon present) was exposed in parallel for each exposure condition.

For tribocorrosion testing, two different solutions were made: 3 g/L NaCl (reference solution) and 80 g/L cassava + 3 g/L NaCl. The addition of NaCl to both solutions was to enhance the conductivity of the electrolyte solution and enable electrochemical measurements.

2.3. Exposure under stirring and static conditions (with and without friction)

Stirring experiments were carried out using acid-washed 12.8 mm × 3.3 mm sized (0.30 g) cylindrical and rounded magnetic stir bars (VWRI442-0366). The stir bars were smaller than the diameter of the glass containers (20 mm) and did not touch the sides of the containers during stirring. They continuously and smoothly had physical contact with the stainless steel coupon, causing friction. The magnetic stirrer (Multistirrer 15) was adjusted to 1500 rpm at room temperature. Stirring was also performed on the blank samples (without any stainless steel coupons) for both the cassava slurry and reference solutions. Both the cassava slurry and reference solutions were stirred for 0.5, 24, and 168 h.

Static experiments were carried out using 20 mL plastic tubes. The coupons were made to stand vertically upright so that both sides of the coupon were exposed, and they were shaken using a VWR Incubating Rocker (shaker) for both the cassava slurry and reference solutions at room temperature. In this setup, there was no friction. The slurry and the

Table 1

Nominal bulk alloy composition of stainless steel grades 304 and 201 based on supplier information (wt%).

Name	UNS	EN (European Norm)	Fe	Cr	Mn	Ni	Cu	Mo	N	C	S
ASTM 201	S20100	1.4372	72.8298	16.9	5.8	3.6	0.4	0.21	0.15	0.11	0.0002
ASTM 304	S30400	1.4301	71.0571	17.9	1.2	9.0	0.4	0.36	0.04	0.04	0.0029

solutions were exposed for 0.5, 24, and 168 h.

After exposure (both stirring and static), the coupons were removed, rinsed with 2 mL of Type I water (the rinsed water was added to the solution to be analyzed), dried with nitrogen gas at room temperature, and placed in a vacuum desiccator before surface analysis. The cassava slurry samples from both stirring and static conditions were frozen before further preparation and analysis. The reference solutions were acidified with ultrapure 65 % HNO₃ to a pH < 2 and stored at room temperature before analysis for preservation.

2.4. Digestion of cassava slurry

Cassava flour is organic; therefore, to prevent hydrogel formation and enable accurate analysis, the cassava slurry samples were digested before trace metal analysis using a microwave digester (Milestone ETHOS UP microwave digesting system). The frozen cassava slurry samples from both stirring and static experiments were thawed. 3 mL of the sample solutions were pipetted into acid-cleaned 5 mL polytetrafluoroethylene (PTFE) digestion tubes containing 333 µL of 65 % ultrapure HNO₃. The temperature was ramped to 170 °C over 10 min and held at 170 °C for 10 additional minutes. The digested samples were allowed to cool to approximately 45 °C. The samples were then transferred into 15 mL centrifuge tubes and diluted to a final volume of 12 mL using Type I water.

2.5. Inductively coupled plasma mass spectrometry (ICP-MS)

The amounts of trace metals released by the metal substrates (ASTM 304 and 201) exposed to the cassava and reference solutions (test media) relative to the blank were measured using inductively coupled plasma mass spectrometry (ICP-MS) with a Thermo Fisher iCAP Q instrument. Here, only specific metal contents (Cr, Fe, Mn, and Ni) predominant within these metal substrates were measured under stirring and static conditions (with and without friction) at 0.5, 24, and 168 h of exposure duration. The metal concentrations within the corresponding blank solutions (c_{blank}), if detectable, were subtracted from the triplicate average of sample concentrations (c_{sample}). The limits of detection, as determined from the background level plus the instrument's detection limit, were 0.060, 0.020, 0.634, and 0.003 µg/L for Cr, Mn, Fe, and Ni, respectively. All calibration curves were linear ($R^2 > 0.9993$) based on a blank and four (Cr) or five (Mn, Fe, Ni) standard concentrations (in 2 % HNO₃) up to 120, 300, 320, and 300 µg/L for Cr, Mn, Fe, and Ni, respectively. Spiked blank samples were run throughout the analyses, and the criteria for re-analysis was a recovery of < 80 % or > 120 %. The amounts of trace metal released (in micrograms per square centimeter) were calculated using Eq. 1.

The exposure volume, V , was 0.005 L for stirring and 0.008 L for static conditions. The surface area, A (cm²), was the geometrical and solution-exposed surface area for the exposed coupon. The dilution factor (DF) is the unitless factor determined from the final volume after digestion divided by the initial sample volume.

$$\text{Amount of metal released } (\mu\text{g}/\text{cm}^2) = \frac{(c_{\text{sample}} \left(\frac{\mu\text{g}}{\text{L}}\right) - c_{\text{blank}} \left(\frac{\mu\text{g}}{\text{L}}\right)) \times \text{DF} \times V}{A \text{ (cm}^2\text{)}} \quad (\text{L}) \quad (1)$$

2.6. Tribocorrosion

Tribocorrosion testing was carried out using a ball-on-plate universal mechanical tester (UMT) Tribolab manufactured by Bruker. ASTM 304 samples were held in a clamp cell with a conductive spring contact on the backside and a solution-exposed surface area of 1.5 cm² sealed by an O-ring in a two-electrode electrochemical cell. The samples were immersed in one of two different electrolytes (80 g/L cassava + 3 g/L NaCl; 3 g/L NaCl). During the test, a 5 mm (diameter) alumina ball slid (linear and reciprocating) against the 304 samples at a speed of 1 mm/s, with a stroke length of 1.5 mm. Experiments were carried out with normal loads of 1 N, 3 N, and 5 N for a duration of 7200 s (2 h). Three replicate tests for each load were carried out, and all the tests were performed at room temperature.

The maximum Hertzian contact stress (σ_c)_{max} [28,29] was calculated by Eqs. 2–3.

$$(\sigma_c)_{\text{max}} = 0.4 \left(\frac{E_*^2 F}{R^2} \right)^{\frac{1}{3}} \quad (2)$$

$$\text{where } \frac{1}{E_*} = \frac{1}{2} \left(\frac{1 - \nu_1^2}{E_1} + \frac{1 - \nu_2^2}{E_2} \right) \quad (3)$$

Where E_1 (300 GPa) and E_2 (200 GPa) are the elastic moduli of alumina ball and ASTM 304 while ν_1 (0.21) and ν_2 (0.29) are the Poisson's ratios of alumina ball and ASTM 304, respectively. F is the normal force (load) in pounds and R (0.0984252 in) is the radius of the alumina ball in inches. The resulting stress in Ksi is then converted to MPa. The calculated maximum Hertzian contact stress at initial contact was 318.4 MPa for 1 N, 459.2 MPa for 3 N, and 544.5 MPa for 5 N.

The specified loads (resulting in different contact stresses), speed, and stroke length were selected for several reasons. The normal loads represented a range of loads starting with a very gentle starting load as judged from the optical microscopy images. The resulting contact stresses represented values between typical load stresses (≥ 670 MPa) and typical shear stresses (≤ 10 MPa) in cassava peeling machines [30, 31]. The speed was chosen to be low enough to not disturb the reference electrode and allow electrochemical measurements. The speed in cassava machines would be expected to be higher; for example, a brush speed of 0.79 m/s was reported previously [32]. Finally, the stroke length of 1.5 mm was the longest possible in the lab-scale tribocorrosion cell setup used (cassava processing machines have a centimeter to meter range of length and movements, [31,33]).

The coefficient of friction (COF) data was smoothed using the oscillating COF calculation parameters of the UMT Test Viewer software. The software's advanced option, which utilizes 50% in the middle of each X-based motion for the frictional force, was selected. The results were then interpolated (UMT Test Viewer) to achieve the desired smoothing. The frictional force and coefficient of friction were measured and recorded by the UMT data acquisition system. In parallel, a

ModuLab XM ECS Solartron potentiostat was used to measure the open-circuit potential, E_{oc} , before (30 min), during (60 min), and after sliding wear tests (30 min). An Ag/AgCl electrode filled with saturated potassium chloride solution was used as the reference electrode, and all potentials in the following are expressed against this reference electrode. To calculate the specific wear rate, Eq. 4 was used to obtain the sliding distance for each sliding time. To obtain the volume loss of the wear tracks, the stainless steel 304 samples were analyzed using a Zeiss confocal laser scanning microscope (LSM800). The depth of the wear tracks was measured within a frame size of 1024 pixels by 1024 pixels at 8 bits per pixel with a pixel dwell time of 4.12 μ s. The C-Epiplan-Apochrome Objective of 20x, NA 0.7 was used, and the pinhole laser aperture was kept at 17 μ m. The wear track was z-stacked at intervals of 0.25 μ m and then tiled across 3 tiles. After the confocal microscope measurement, the results were analyzed using Zeiss ConfoMap software (version 7.4.8341). The images were first levelled and their thresholds were adjusted. Then, the depth of the wear tracks was evaluated using the average north-to-south profiles of the wear track images. The wear track's cross-section was determined using the area of the hole function within the ConfoMap software. This cross-section was then multiplied by the length of the wear track (1.5 mm) to obtain the volume loss. Eq. 5 [34] was used to determine the specific wear rate.

$$\text{Sliding distance (m)} = \text{time (s)} \times \text{velocity (m/s)} \quad (4)$$

$$\text{Specific wear rate (m}^3/\text{m} \times \text{N)} = \frac{\text{Volume loss (m}^3\text{)}}{\text{sliding distance (m)} \times \text{normal load (N)}} \quad (5)$$

KaleidaGraph v.4.0 software was used for linear fitting and the specific wear rates were obtained from the slopes of the volume loss vs. (sliding distance \times normal load) curve.

2.7. Microscopic analysis

After the stirring (friction induced by a stir bar) and static conditions, and after the tribocorrosion testing, the coupons (ASTM 304 and 201 stainless steels) were rinsed, dried, and stored in a desiccator with < 10 % relative humidity. Any changes in their surface morphology, in comparison to unexposed reference coupons, were examined using a Keyence VHX-6000 optical microscope (OM) and a Hitachi SU3500 scanning electron microscope (SEM) coupled with energy dispersive X-ray spectroscopy (EDX). An accelerating voltage of 10–15 kV was used for the analyses.

2.8. X-ray photoelectron spectroscopy (XPS)

The surface composition of the ASTM 304 stainless steel samples after tribocorrosion testing was also analyzed using X-ray photoelectron spectroscopy (Kratos AXIS Supra Spectrometer). One coupon for each solution (NaCl reference or NaCl + cassava slurry solutions) and two loads (3 and 5 N) were measured at two locations (within and outside of the wear track), resulting in 8 measurements. A monochromatic Al K_{α} source (15 mA, 15 kV) was used, and the instrument's work function was calibrated to give a binding energy (BE) of 83.96 eV for the Au 4 $f_{7/2}$ line for metallic gold and the spectrometer dispersion was adjusted to give a BE of 932.62 eV for the Cu 2 $p_{3/2}$ line of metallic copper. The Kratos charge neutralizer system was used on all specimens. All specimens were electrically isolated from the instrument sample holder for these analyses. For measurements outside the wear track, survey scans were carried out with an analysis area of 300 \times 700 μ m and a pass energy of 160 eV and high-resolution analyses were carried out with an analysis area of 300 \times 700 μ m and a pass energy of 20 eV. For measurements inside the wear track (in the middle of it), a smaller spot size of 110 μ m diameter was used. High-resolution spectra for C 1 s, O 1 s, Fe 2p, Cr 2p, and Ni 2p were collected. High-resolution spectra were charge-corrected according to the main line of adventitious carbon

(284.8 eV) [35]. Further, Fe 2p, Cr 2p, and Ni 2p spectra were deconvoluted using fitting parameters reported previously [36,37]. All spectra were analyzed using CasaXPS software (version 2.3.23).

2.9. Statistical analysis

A student's t-test for unequal variance and unpaired data was used to compare two different datasets of independent samples for two different conditions. If the probability (p) that these datasets were smaller than 0.05, it was deemed to be a statistically significant difference. For calculations, KaleidaGraph v.4.0 software was used.

3. Results and discussion

3.1. Metal release

The released amounts of metals (Cr, Fe, Mn, and Ni) into the cassava slurry in stirred (a) and static (b) conditions and reference solution in stirred (c) and static (d) conditions from 304 and 201 stainless steel coupons after 0.5, 24, and 168 h exposure at room temperature are presented in Fig. 1. Stirred conditions mean that the magnetic stir bar induced friction, while static conditions were without friction. The greatest amount of metal was released into cassava slurry in stirred conditions (168 h: 49–59 μ g Fe/cm², 11–14 μ g Cr/cm², 3–6 μ g Ni/cm², and 0.8–5 μ g Mn/cm² for 201 and 304 stainless steels), followed by the reference solution (water) under stirring, cassava slurry in static conditions, and reference solution in static conditions (168 h: <0.23 μ g/cm² for any metal). It was clear that the combined effect of cassava and friction was synergistic. When comparing the stirred cassava with the stirred water (reference) solution, the release of metals was significantly higher (168 h: the total, Fe+Cr+Ni+Mn, release was 12-fold higher for 304 and 4-fold higher for 201 stainless steel). The difference was obvious for all metals, although most pronounced for Fe (both stainless steels, 11–83-fold higher in cassava than the water reference solution) and for Cr for 304 stainless steel (242-fold increase due to the presence of cassava). When comparing the stirred cassava with the static (no friction) solution, the increase was 30–35-fold for the total metal release for both stainless steels after 168 h, with differences most obvious for Cr release (1168-fold increase for 304 and 691-fold increase for 201 stainless steel due to the friction).

It has been reported [17] that under passive conditions (no active or localized corrosion), the Fe release from these stainless steel grades makes up more than 90 % of the total release, while Ni and Cr release are more pronounced during active or localized corrosion conditions. In stirred conditions (Fig. 1, both solutions), the relative percentage of Fe release of the total metal release decreased from more than 86 % to 11–73 % and 26–72 % of the total release from 304 and 201 stainless steel, respectively. In comparison, in static conditions (without friction), the relative percentage of Fe release reached 78–92 % after one week of exposure.

Consequently, the released amounts of Cr and Ni were not negligible in comparison to the total release after 168 h in all solutions in stirred conditions. The relative release of Ni, as part of the total release, from 304 and 201 into stirred reference (water) solution increased from 4 % to 25% (201) and 77 % (304) with time, from 0.01–0.02 μ g Ni/cm² to 4.2–4.9 μ g Ni/cm² for both stainless steels. In stirred cassava, the percentage of Ni release did not increase to more than 9% (304) and 4 % (201) but reached similar absolute values after 168 h, of 3.5–6.2 μ g Ni/cm². Cr, on the other hand, increased from 2–3 % to 16–17 % of total release from 304 and 201 in cassava slurry in stirred conditions (from 0.01–0.04 μ g Cr/cm² to 11–14 μ g Cr/cm²) with exposure time, whereas in the reference solution, the relative Cr release increased only slightly from 1 % to 1–3 % of total release in stirred conditions and remained below 0.6 μ g Cr/cm² after 168 h for both stainless steels. It is likely that the relatively high Ni release and relatively low Cr release in the reference solution (water) in stirred conditions is caused by destruction of the

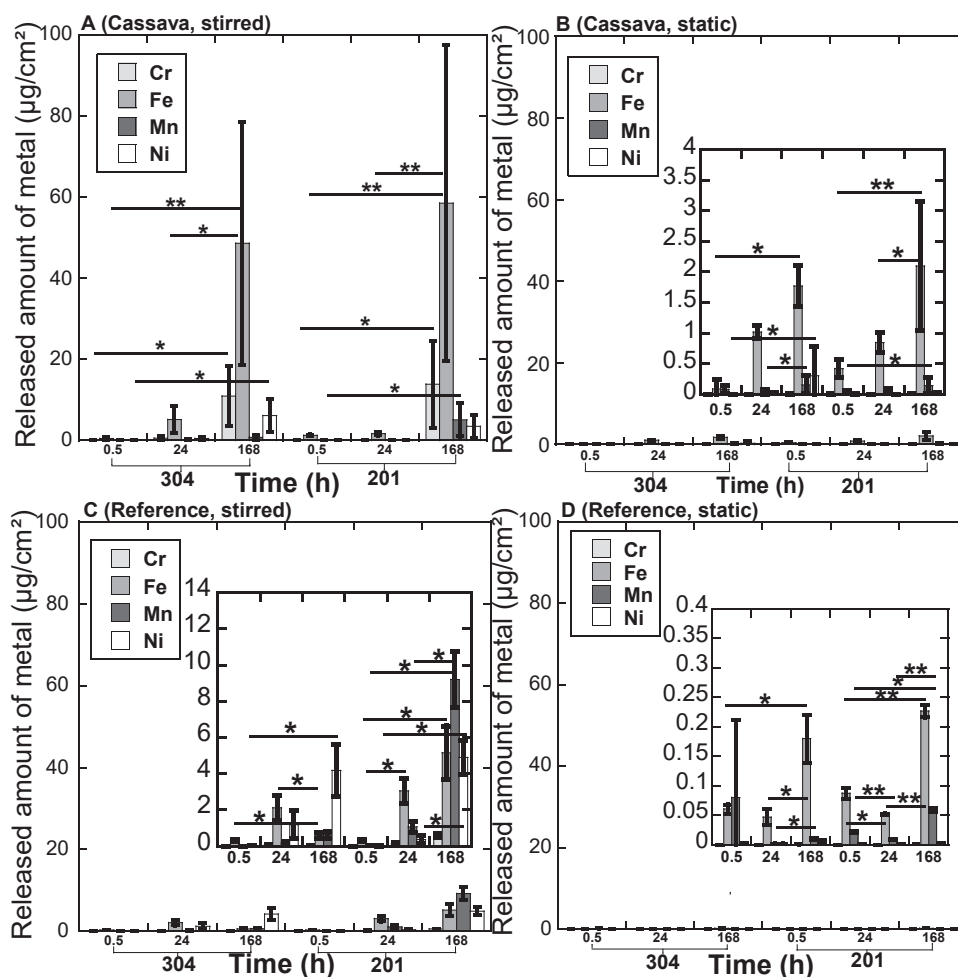


Fig. 1. Released amounts of metals (Cr, Fe, Mn, and Ni) from 304 and 201 stainless steel coupons into cassava slurry and reference (water) solution after 0.5, 24, and 168 h in stirred and static conditions at room temperature. Error bars show the standard deviation among independent triplicate samples. Insets show magnified datasets. Asterisks indicate statistically significant (* means $p < 0.05$; ** means $p < 0.01$) differences between the two time points of the same element.

surface oxide (activation due to friction) and subsequent precipitation of Cr oxides, as Cr is not soluble in neutral water while Ni is [38].

This indicates active and/or localized corrosion induced by the combination of chemical effects and mechanical action (the stir bar sliding over the coupon). In all cases, the released amounts of metals were higher (on average, a 24-fold increase) in stirred compared with static conditions. The different ratios of metals released in water and

cassava under stirring indicate different degradation mechanisms. Although there was a higher release from 201 stainless steel compared with 304 stainless steel, the difference was not statistically significant.

Changes in surface appearance with time observed through scanning electron microscopy (SEM) on the 304 and 201 stainless steel coupons after exposure to the cassava slurry and the reference solution under stirring and static conditions are presented in Fig. 2. Under static

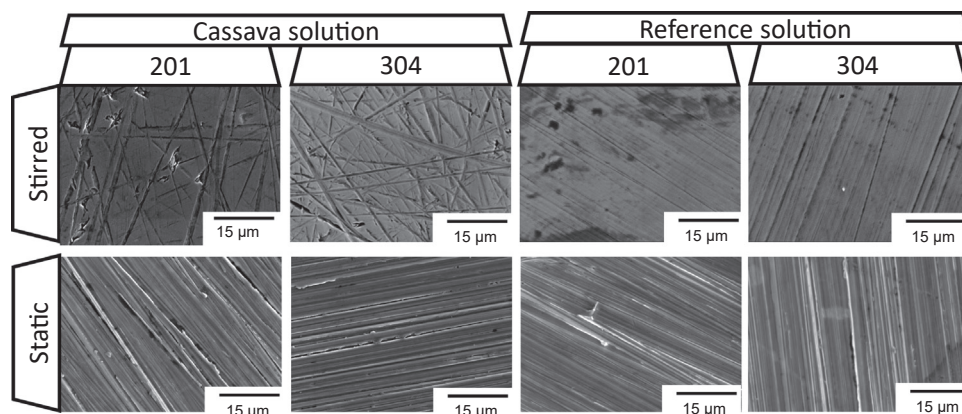


Fig. 2. SEM images of representative metal coupons exposed under stirred and static conditions at room temperature in the cassava slurry and reference (water) solution for 24 h. More details in Fig. S1.

conditions, only the grinding lines (all parallel) were visible on the surfaces in both solutions (cassava and reference solutions). However, under stirring (with friction induced by the stir bar), there was a clear difference between the two solutions; in the presence of cassava, scratches were visible in all directions, while the scratches in the reference solution were still parallel, indicative of far less surface damage. In the reference solution under stirring, there were also some patches and pits visible, indicative of some oxidative wear and three-body abrasive wear, possibly caused by wear debris over time. In contrast, the cassava slurry induced three-body abrasive wear from the beginning, which caused grooves and pits (Fig. 2), which are a consequence of three-body abrasive wear [39]. Also, there were fewer patches or indications of oxidative wear in the cassava slurry, as it almost looked polished, possibly indicating a chemical etching effect. Another explanation could be fatigue abrasive wear that prevails when a material is exposed to cyclic loading [40].

3.2. Tribocorrosion results

Fig. 3 shows the open circuit potential E_{oc} of 304 stainless steel samples in the NaCl reference solution and cassava + NaCl solution before, during, and after tribocorrosion tests. The potential values stabilized during the first 30 min before the load was applied to the samples, to approximately -110 to -130 mV vs. Ag/AgCl sat. KCl (Table 2). When the ball started to slide on the surface of the sample, a sudden decrease in the potential values was observed, indicating the destruction of the passive film and activation of the material inside the wear track [41]. The potential drop was highest when a normal load of 5 N (dropping to -230 to -250 mV) was applied to the surface of the samples, followed by 3 N (to -203 mV) and 1 N (to -155 to -182 mV) in both solutions, Fig. 3 and Table 2. During continuous sliding, the potential remained relatively constant at that lower value in the reference solution (only NaCl, Fig. 3a). This indicates an equilibrium of activation and repassivation events during the sliding period [42]. In the cassava + NaCl solution (Fig. 3b), the potential decreased slightly during the sliding period, indicative of further activation or less repassivation. After the load was released from the samples (after 90 min), the potential values returned to approximately their initial values in NaCl solution (-100 to -130 mV), Fig. 3a and c and Table 2, which is evidence that the oxide film was reformed (complete repassivation process of the wear track). However, for the cassava + NaCl solution, the potential values did not revert to the initial values (-140 to -220 mV), indicating that the passivation was incomplete. The difference between the potential drop after 30 min (ΔE_1) and the potential increase after 90 min (ΔE_2) was highest for the load of 5 N in the cassava + NaCl solution, followed by 3 N and then 1 N, Fig. 3b and d. In the following, some tribological results are presented. These are discussed together with the other results in Section 2.4.

For each solution and normal load, the volume loss vs. sliding distance \times normal load was plotted [34], and the results are shown in Fig. 4. The volume loss, estimated from confocal microscopy, was smaller for the cassava solution due to better lubrication (see below),

Table 2

Average potentials (and standard deviations of triplicate samples) of 304 stainless steel achieved before, during and after sliding (examples shown in Fig. 3). Potentials are shown against the reference electrode of Ag/AgCl sat. KCl.

Normal Load	Before sliding	During sliding	After sliding
Cassava + NaCl solution			
1 N	-122 ± 0.6 mV	-155 ± 10.4 mV	-136 ± 8.3 mV
3 N	-128 ± 0.5 mV	-203 ± 17.4 mV	-177 ± 10.4 mV
5 N	-108 ± 3.8 mV	-249 ± 35.4 mV	-217 ± 15.4 mV
NaCl solution			
1 N	-109 ± 0.6 mV	-182 ± 11.4 mV	-98 ± 7.4 mV
3 N	-108 ± 1.1 mV	-203 ± 13.6 mV	-112 ± 18.6 mV
5 N	-111 ± 0.6 mV	-227 ± 18.0 mV	-129 ± 17.8 mV

Fig. 4. The slopes of a linear fit, which represent the specific wear rates, of the two curves for NaCl and cassava + NaCl were similar ($1.27 \cdot 10^{-14} \text{ m}^3/(\text{m} \times \text{N})$).

Wear track images of 304 stainless steel samples imaged by OM and examples of cross sections determined by confocal microscopy after tribocorrosion testing at three different loads in two different solutions are shown in Fig. 5. Sliding in cassava + NaCl solution resulted in shallower but wider wear tracks compared to NaCl solution. Significant plastic deformation and abrasion [43] was found for the load of 5 N in cassava + NaCl solution, Fig. 5.

The COF versus time curve and mean values of COF obtained over a 60-minute period of load application are shown in Figs. 6a and 6b, respectively. The COF values for 304 stainless steel samples in cassava + NaCl solution were significantly lower than in the NaCl reference solution (for all loads). The COF vs. time curve for cassava + NaCl solution appears to be noisier compared to the smoother curve of the NaCl solution. It was also observed that in the NaCl solution, the initial (first 10 min) COF values decreased with a higher applied load. Furthermore, for 1 N and 3 N loads in NaCl solution, the COF values decreased over time. However, for the load of 5 N in NaCl solution, the COF value was relatively constant throughout the 60 min of sliding.

The wear tracks were further imaged by SEM, Fig. 7. For loads of 3 and 5 N in the cassava + NaCl solution, signs of abrasive three-body wear and adhesive wear (smeared out areas) were visible. EDX analysis indicated a similar or higher oxygen content outside of the wear track compared to inside the wear track for the NaCl reference solution, whereas this relation was reversed for the cassava + NaCl solution for the higher loads of 3 and 5 N, Fig. 8.

3.3. Surface analysis inside and outside the wear track

The relative atomic percentage and speciation of Cr, Fe, and Ni in the surface oxide and alloy beneath the surface oxide inside and outside the wear track for 304 samples in both NaCl and cassava + NaCl solutions are shown in Fig. 9a. It was observed that there was a higher $\text{Cr}(\text{OH})_3$ fraction in the wear track of the 304 samples for both loads 3 N and 5 N in cassava + NaCl solution compared to outside the wear track and the NaCl solution. An opposite trend was found for the relative atomic percentage for Cr_2O_3 (lowest inside the wear track of cassava + NaCl solution). This is due to the active dissolution and corrosion events occurring in the wear track after the destruction of the passive film layer [44,45]. It should be emphasized that all surfaces in this study still remained passive, as indicated by the presence of metallic signals from XPS in all cases (Fig. 9a), meaning that the surface oxide is thinner than the instrument's information depth of 7–10 nm in all cases. Fig. 9b shows the relative Cr content in the oxide. Generally, corrosion and repassivation events result in higher Cr enrichments in the surface oxide [46,47]. Negligible Cr enrichment was only found for the NaCl solution outside of the wear track for an applied load of 3 N, Fig. 9b. For all loads and solutions, Cr enrichment was higher inside the wear track than outside of it, Fig. 9b. This is expected from literature findings on the effect of ball milling on surface Cr enrichment of stainless steel [48]. Further, in agreement with the EDX results (Fig. 8), the fraction of oxidic to metallic peaks for Fe, Cr, and Ni (Fig. 9a) showed that the oxide was thicker inside the wear track than outside of it for the cassava + NaCl solution, but the opposite (thicker outside of the wear track than inside it) for the NaCl reference solution. This indicates active corrosion in the wear track in the cassava + NaCl solution for both loads, and a faster repassivation ability for the NaCl compared to cassava + NaCl solution.

3.4. Further discussion

There was a higher metal release from both 304 and 201 stainless steels (on average, 22-fold) into cassava slurry and water reference solutions for stirring conditions (with mechanical contact to a stir bar) compared to static conditions. Also, the tribocorrosion results showed a

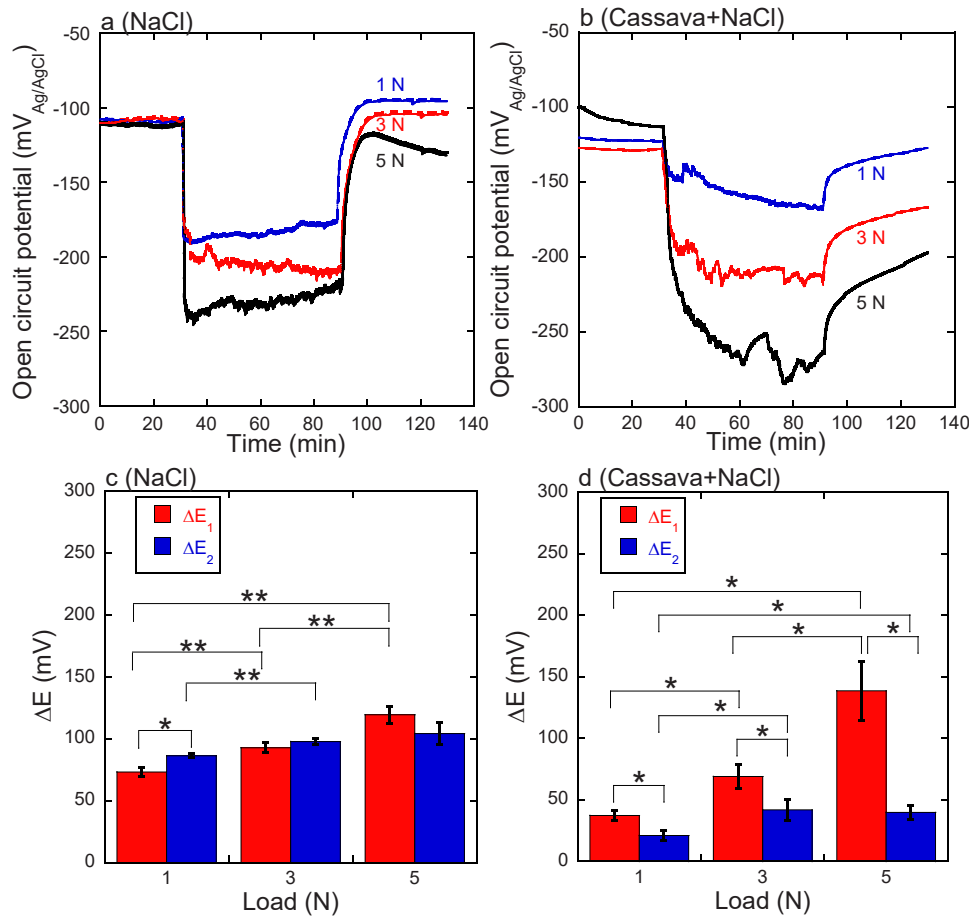


Fig. 3. Representative open circuit potential (mV) vs. Ag/AgCl sat. KCl curves over time on ASTM 304 stainless steel samples in (a) 3 g/L NaCl reference solution and (b) 80 g/L cassava + 3 g/L NaCl at room temperature, whereas the first 30 min, no load was applied, followed by sliding with 1 N, 3 N, or 5 N load for 60 min, followed by no load application for 30 min. The potential drop after 30 min (ΔE_1) and the potential increase after 90 min (ΔE_2) for three replicate measurements (error bars show the standard deviation between them) are plotted in (c) NaCl and (d) cassava + NaCl. Asterisks indicate statistically significant differences between two time points or two different loads (* means $p < 0.05$; ** means $p < 0.01$).

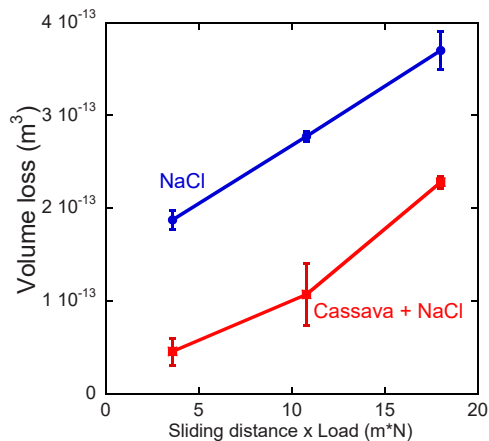


Fig. 4. Volume loss versus (sliding distance × normal load) curve for 304 stainless steel samples in 3 g/L NaCl reference solution and 80 g/L cassava + 3 g/L NaCl during sliding with 1 N, 3 N, or 5 N load for 60 min. The error bars show the standard deviation of triplicate samples. The connecting lines are only guidance for the eye. The slope represents the specific wear rate.

clear dependence on the applied load. This highlights the potential impact of friction on the release of metals from the stainless steel surface into food (cassava slurry) and reference solutions. A previous study on

metal release from stainless steel into whey protein solution using a similar experimental setup with a stir bar also found that the released amounts of metals were higher (on average, an 8-fold increase) in stirred conditions compared with static conditions [15]. Under stirred conditions in the cassava slurry, 304 and 201 stainless steels released significantly more Cr and Ni than in the static condition, especially after 168 h. This means that the friction damaged the passive layer of the stainless steels [50]. In cassava slurry, the degradation of the passive surface oxide might further be exacerbated by the presence of hydrogen cyanide [51]. This can be particularly detrimental if regularly reoccurring and for foods that contain components that hinder the repassivation of the surface oxide of stainless steel. This hindrance of repassivation was reported in this study and also in a previous study on stainless steel in the presence of whey proteins after several days of friction induced by a stir bar [52].

Further, the amount of metal that was released from 304 and 201 stainless steels into the cassava slurry was much higher (on average, a 35- and 9- fold increase in stirred and static conditions, respectively) than the amount that was released in the reference solution. Likewise, there was a greater potential drop and slower repassivation of 304 in the presence of cassava compared to the absence of it in the tribocorrosion investigations. Food and its preparation can be corrosive due to various halides, chlorides, complexing agents, high and low pH [14]. The cassava slurry exhibits a slightly higher acidity (pH 5.6) than the reference solution, which has a natural pH equivalent to water, but this difference is negligible for stainless steels. The higher release of metals from

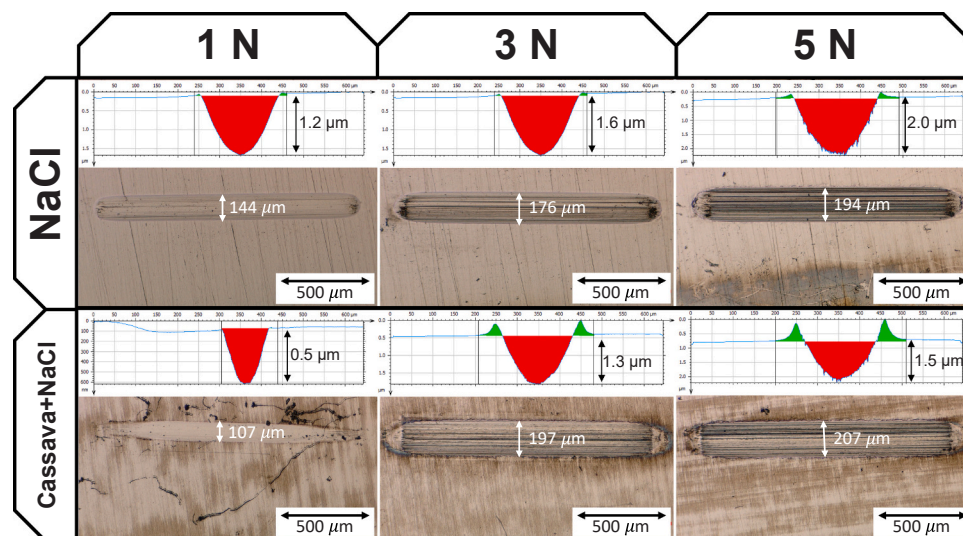


Fig. 5. Examples of wear tracks on 304 stainless steel samples images imaged by optical microscopy after tribocorrosion in 3 g/L NaCl reference solution (top) and 80 g/L cassava and + 3 g/L NaCl (bottom) at room temperature for 2 h (1 h under load) for different sliding with 1 N, 3 N, or 5 N load. Insets show examples of the cross-section profiles of the wear tracks, imaged by confocal microscopy.

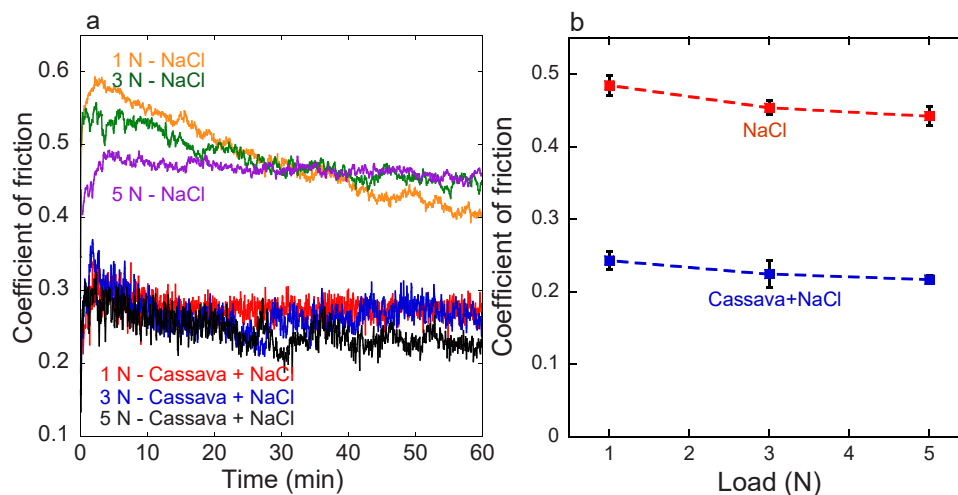


Fig. 6. Representative coefficient of friction vs. time curves in 3 g/L NaCl reference solution and 80 g/L cassava + 3 g/L NaCl at room temperature during sliding on 304 stainless steel samples with 1 N, 3 N, or 5 N load applied for 60 min (a). Mean values of the coefficient of friction during the 60 min load application for three independent samples with the error bars showing the standard deviation (b).

stainless steel into a cassava slurry and the larger potential drop in the tribocorrosion measurements in cassava solution compared with the reference solutions can be explained by several factors related to the composition of the cassava slurry, the presence of complexing agents, and the nature of the interface between the stainless steel and the slurry. Compared to stainless steel exposed to the reference solutions, metal-organic complexes can increase the solubility of metals [38,53,54], which can either result in slow surface oxide dissolution processes [55,56] or, in this case, in slower repassivation (the oxide is less stable), which results in higher release of metals. A previous study [52] used a similar experimental setup and found total (Fe, Cr, and Ni) metal release values of $< 3 \mu\text{g}/\text{cm}^2$ after 24 h and $22 \mu\text{g}/\text{cm}^2$ after 72 h from stainless steel 316 L in stirred phosphate buffered saline containing 10 g/L whey protein. In this study, the total metal release from 304 and 201 in 80 g/L cassava slurry was $< 7 \mu\text{g}/\text{cm}^2$ (24 h) and $< 81 \mu\text{g}/\text{cm}^2$ (168 h). This means that the cassava solution in this study is more corrosive than the whey protein-containing solution, or grades 304 and 201 were more corrosion-susceptible than 316 L. Both studies show accelerated metal release after several days of stirring.

In this study, 201 stainless steel released slightly more metals (not statistically significant) than 304 stainless steel. Previous studies found that the release of metals from stainless steel is influenced by various factors, including the surface finishing and solution composition [57,58]. It was also found that the release rates of Cr, Ni, and Fe from stainless steels are generally lower than those of pure iron or nickel due to the protective Cr-rich surface oxide [59]. These and other [17] studies collectively suggest that while 201 stainless steel may release slightly more metals than 304 stainless steel, the difference was negligible. 201 stainless steel contains more Mn and less Ni compared to 304 stainless steel. Also, 304 stainless steel typically contains a higher Cr content than 201 stainless steel (as also in this study). Cr forms a Cr-rich oxide layer on the surface, which is stable and protective in benign conditions [60], preventing the release of metal ions into surrounding environments. The higher Ni content in 304 improves the resistance of stainless steel to various forms of corrosion, including pitting and crevice corrosion [61]. However, pitting and crevice corrosion were not the dominant corrosion and wear mechanisms in this study (no evidence of pits or localized corrosion was found in this study). Therefore, it is not surprising that

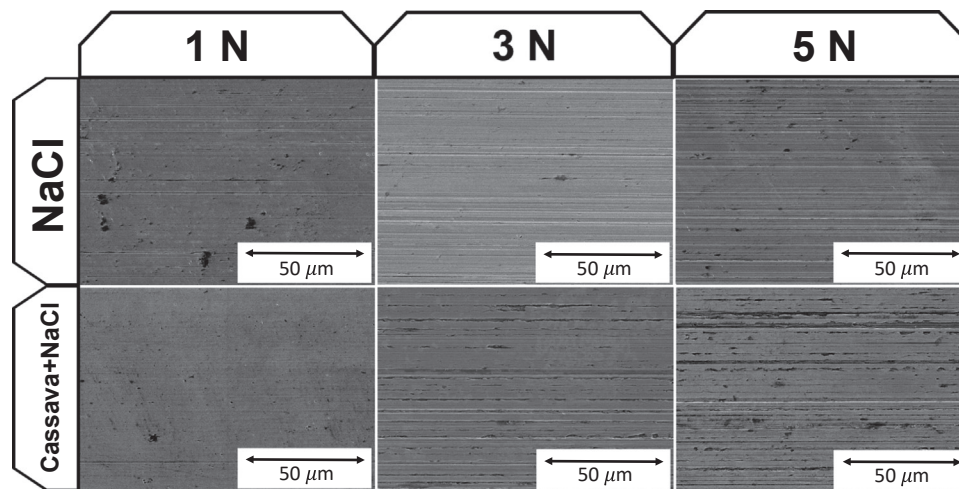


Fig. 7. Examples of interior sections within the wear tracks on 304 stainless steel samples imaged by SEM after tribocorrosion in 3 g/L NaCl reference solution (top) and 80 g/L cassava + 3 g/L NaCl (bottom) at room temperature for 2 h (1 h under load) for sliding with 1 N, 3 N, or 5 N load.

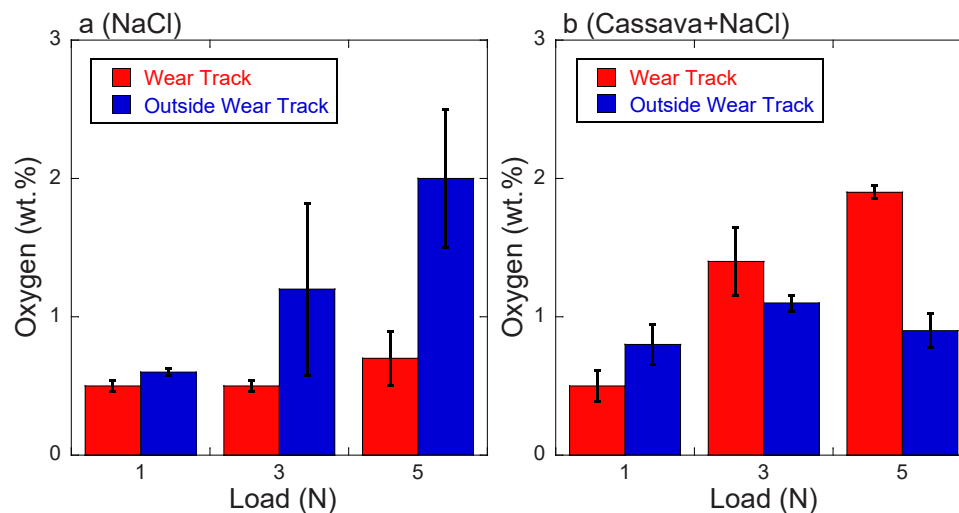


Fig. 8. Oxygen weight percent measured on 304 stainless steel samples by EDX after tribocorrosion in 3 g/L NaCl reference solution (left) and 80 g/L cassava + 3 g/L NaCl (right) at room temperature for 2 h (1 h under load) for sliding with 1 N, 3 N, or 5 N load. The error bars show the standard deviation of three measurements on each of the wear track and outside the wear track on 304 samples.

there was a negligible difference in metal release between 201 and 304 in this study.

In this study, the specific wear rate, which considers the expected increase in volume loss with the sliding distance and normal load [34, 62], of 304 stainless steel was the same for both NaCl and cassava + NaCl, which was caused by two opposing trends: 1) higher corrosion in cassava + NaCl, and 2) lower coefficient of friction in the presence of cassava, than in the absence of cassava. The higher corrosion in the presence of cassava compared to the NaCl solution was proven by 1) a larger potential drop on the onset of sliding and a smaller increase of potential after the sliding process (less ability to reform the oxide), 2) higher metal release, and 3) a higher oxygen content, thicker oxide, and higher $\text{Cr}(\text{OH})_3$ content in the wear track. The lower COF in the presence of cassava compared to its absence was evident for all normal loads investigated. This could be caused either by slurry particles or wear debris, which could reduce the area of contact [63], or by a lubrication effect. Third-body wear (caused by particles) is evident for both solutions from the SEM images and is indeed more evident for cassava + NaCl compared to NaCl solution for 3 and 5 N normal loads (Fig. 7). The presence of particles in cassava + NaCl slurry is also visible from the noisy COF over time curves in this solution (Fig. 6). However, since the

COF in cassava + NaCl compared to NaCl solution was also significantly lower at 1 N normal load but there were no signs of third-body wear in the corresponding SEM images, in contrast to NaCl solution, lubrication must at least have played a role in lowering the COF. Also, the SEM images from the stir bar experiments (Fig. 2 and S1) indicate oxidated patches only in the absence of cassava. Oxidated wear debris patches would reduce the contacting area. Instead, the presence of cassava caused a chemical polishing effect and no signs of any build-up of wear debris (Fig. 2 and S1). Yet another indication that lubrication might be more important than wear product build-up, and consequently a reduction in the area of contact, for the cassava + NaCl solution were the COF over time curves (Fig. 6), which decreased with time for the NaCl solution, but not for the cassava + NaCl solution. While the specific wear rate was the same between the two solutions, the total volume loss was lower for cassava + NaCl than for the NaCl solution, and the wear tracks were shallower but wider in the presence of cassava. Cassava is known to be a lubricating material because the amylose content present in cassava allows its starch to function similarly to viscosity-enhancing and fluid-loss control polymers [64].

The combined action of friction and the presence of cassava was synergistic (more than a simple additive effect) for the resulting metal

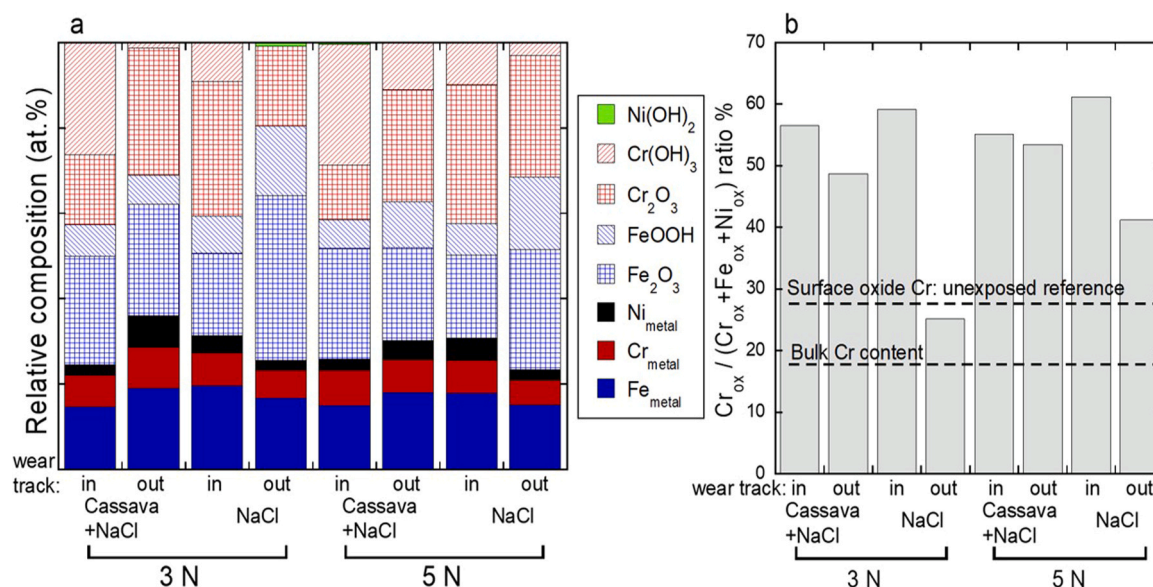


Fig. 9. The relative atomic percentage and speciation of Cr, Fe, and Ni in the surface oxide and alloy beneath the surface oxide inside (“in”) and outside (“out”) the wear track (one spot each) for 304 samples after tribocorrosion exposures to both NaCl and cassava + NaCl solutions at 3 and 5 N load at room temperature (a). The corresponding atomic ratio percentage of oxidic Cr to oxidic Cr, Fe and Ni (b). The two dashed lines in (b) indicate the bulk Cr content and the previously reported [49] corresponding surface ratio for unexposed 304 surfaces.

release. The combined action of friction and cassava caused a significant increase in the sum of the release of Fe, Cr, Ni, and Mn from the stainless steels (30–35-fold increase compared to no friction, and 4–12-fold increase compared to water without cassava but with friction). The sum of the metal release in cassava + NaCl solution (without friction) and the reference water solution (with friction) is 7.7 $\mu\text{g}/\text{cm}^2$ for 304 and 22 $\mu\text{g}/\text{cm}^2$ for 201, as compared to the actually measured 67 $\mu\text{g}/\text{cm}^2$ for 304 and 81 $\mu\text{g}/\text{cm}^2$ for 201 in cassava + NaCl solution with friction. Since 67–81 $\mu\text{g}/\text{cm}^2$ is greater than 7.7–22 $\mu\text{g}/\text{cm}^2$, the effect of friction and cassava is not simply additive but synergistic for both stainless steel grades.

In total, despite relatively high amounts of released metals (for stainless steel), the surface retained its ability to re-passivate, as indicated by the XPS results. The results could have been worse if recycled scrap cookware materials had been tested [65]. A previous study focused on the elevated risk of metal exposure among individuals working at informal foundries, emphasizing the impact of environmental and occupational exposure in relation to facility formalization and regulatory compliance. The study found that informal foundries pose higher risks due to rudimentary structures, minimal use of protective equipment, and lack of regulatory compliance. Elevated blood lead (Pb) concentrations in artisanal pot makers confirm that informal foundries are occupational sources of Pb and other toxic metals. Informal foundries located in residential areas pose risks to entire communities, especially vulnerable groups such as children and pregnant women [65]. In addition, it was previously found that water boiled in locally crafted cookware had the highest concentrations of potentially toxic metals, followed by aluminum cookware and, lastly, stainless-steel cookware [66]. These findings indicated that the utilization of locally made cookware exposes boiled water and food to metal contamination, particularly when harsh cleaning materials are employed. The potentially toxic metals, like Pb, likely originated from metal scrap, the primary raw material used by local artisans in cookware fabrication in Africa. Unfortunately, these components are often inadequately alloyed and lack anodization, making the cookware susceptible to corrosion by water, salt, and various environmental agents. One study [67] identified that water boiled in locally fabricated cookware exhibited elevated levels of aluminum (Al) ($114.0 \pm 0.2 \mu\text{g}/\text{mL}$), followed by Pb ($90.0 \pm 8.0 \mu\text{g}/\text{mL}$), and cadmium (Cd) ($58.0 \pm 3.0 \mu\text{g}/\text{mL}$). These

concentrations far exceeded the permissible limits set by the World Health Organization (WHO) for heavy metals. The high Al levels were attributed to the prevalent use of scrap materials derived from discarded Al products, such as plates, motor parts, old Al pots, broken spoons, and cans. That study [67] aligns with other research [65,68], indicating exposure hazards to Pb, Al, and Cd from locally fabricated cookware.

This study is limited by the use of chemically complex cassava flour, which disables the identification of active and corrosive components, and the use of high-quality stainless steel rather than relevant local stainless steel. Further studies should also investigate the effect of temperature and other food components. In addition, future studies utilizing applied potentials to distinguish between mechanical and chemical wear by applying reductive and oxidative potentials are encouraged. Further, other tribocorrosion setups could be applied, which more closely mimic stainless steel processing machine speeds, forces, and geometric parameters. While the Hertzian contact pressure in this study (318.4–544.5 MPa) aligns well with other ball-on-plate tribometer setups, for example, 593.4 MPa in a study done by [34], it is far greater than expected shear stress in cassava peeling machines. Depending on the blade diameter and the moisture content in the cassava tubers, these range between 0.65 and 9.25 MPa [31]. On the other hand, these machines are also exposed to large load stresses (670–809 MPa, [30]), high speeds (1550 rpm in [30]), and fatigue, which necessitates further investigations in the context of potential synergistic mechanical and corrosion degradation modes.

4. Conclusions

This study investigated the influence of cassava flour on metal release from two common food contact stainless steels, ASTM 304 and 201, during stirring and static conditions (with and without friction) and the tribocorrosion of stainless steel 304 in the presence and absence of cassava. The following main conclusions are drawn:

1. Mechanical friction increased the metal release and the extent of electrochemical corrosion in the presence and absence of cassava.
2. Relatively high amounts ($<81 \mu\text{g}/\text{cm}^2$) of Fe, Cr, Ni, and Mn were released into cassava slurry under the action of a stir bar in mechanical contact during 168 h at room temperature.

- The effect of both friction and cassava on metal release was synergistic after 168 h of exposure (30–35-fold increase in total metal release compared to no friction, and 4–12-fold increase compared to water without cassava but with friction).
- Cassava hindered the re-passivation of the surface oxide of stainless steel 304.
- Tribocorrosion in the presence of cassava resulted in a higher Cr enrichment and a higher fraction of Cr(OH)₃ in the surface oxide.
- Cassava acted as a lubricant, reducing the coefficient of friction. This resulted in shallower, but wider, wear tracks than in the reference solution (NaCl solution), due to the combined effect of corrosion and lubrication.

Statement of originality

This research is original and novel. To the best of our knowledge, no tribocorrosion study has been published on stainless steel in cassava food environments. No part of this study has been published elsewhere, and this paper, or parts of it, is not submitted elsewhere for publication.

CRediT authorship contribution statement

R. Addai: Writing – original draft, Validation, Visualization, Methodology, Investigation, Formal analysis. **T.E. Olowoyo:** Writing – original draft, Validation, Visualization, Methodology, Investigation, Formal analysis. **J.D. Henderson:** Writing – review & editing, Investigation. **T.E. Standish:** Writing – review & editing, Investigation. **U. Eduok:** Writing – review & editing, Validation. **Y.S. Hedberg:** Writing – review & editing, Validation, Visualization, Resources, Project administration, Supervision, Methodology, Funding acquisition, Formal analysis, Conceptualization.

Funding

This work was supported by the Wolfe-Western fellowship, Canada [grant number 2020]; Canada Research Chairs Program [grant number: CRC-2019-00425], and the Natural Sciences and Engineering Research Council of Canada [grant numbers DGDND-2021-03997, RGPIN-2021-03997, RGPIN-2020-06856].

Declaration of Competing Interest

The authors declare the following financial interests/personal relationships which may be considered as potential competing interests: Yolanda Hedberg reports financial support was provided by Natural Sciences and Engineering Research Council of Canada. Yolanda Hedberg reports financial support was provided by Western University. Yolanda Hedberg reports financial support was provided by Canada Research Chairs Program. If there are other authors, they declare that they have no known competing financial interests or personal relationships that could have appeared to influence the work reported in this paper.

Data Availability

Data is shared on https://osf.io/gukf4/?view_only=a3c49791d06146ca99e9434188b59d59.

Acknowledgements

We thank Dr. Jonas Hedberg for help with the inductively coupled plasma mass spectrometry, Dr. Zheng Wei for the initial training of the metal release tests, Dr. Sina Matin for the initial training on the tribocorrosion system, and Drs. Ivan Barker and Vahid Dehnavi (all of these at the University of Western Ontario) for training on the scanning electron and confocal microscopes. We also acknowledge the first-year report examination committees of the Department of Chemistry,

University of Western Ontario.

Appendix A. Supporting information

Supplementary data associated with this article can be found in the online version at [doi:10.1016/j.triboint.2024.109656](https://doi.org/10.1016/j.triboint.2024.109656).

References

- Alves AAC. Cassava botany and physiology. In: Hillocks RJ, Thresh JM, Bellotti AC, editors. Cassava: biology, production and utilization. CAB International; 2002. p. 67–89.
- Zhu F. Composition, structure, physicochemical properties, and modifications of cassava starch. *Carbohydr Polym* 2015;122:456–80. <https://doi.org/10.1016/j.carbpol.2014.10.063>.
- FAOSTAT (2019). Cassava production in 2018, Crops/World Regions/Production Quantity from pick lists. (<https://www.fao.org/faostat/en/#data>).
- Bayata AJ. Review on nutritional value of cassava for use as a staple food. *Sci J Anal Chem* 2019;7(4):83–91. <https://doi.org/10.11648/j.sjac.20190704.12>.
- Westby A. Cassava utilization, storage and small-scale processing. Cassava: biology, production and utilization. UK: Cabi Wallingford.; 2001. p. 281–300.
- Olomo V, Ajibola O. Processing factors affecting the yield and physicochemical properties of starch from cassava chips and flour. *Starch - Stärke* 2003;55(10): 476–81. <https://doi.org/10.1002/star.200300201>.
- Charoenkul N, Uttapap D, Pathipanawat W, Takeda Y. Physicochemical characteristics of starches and flours from cassava varieties having different cooked root textures. *LWT - Food Sci Technol* 2011;44(8):1774–81. <https://doi.org/10.1016/j.lwt.2011.03.009>.
- Adekanye TA, Ogunjimi SI, Ajala AO. An assessment of cassava processing plants in irepodun local government areas, Kwara State, Nigeria. *World J Agric Res* 2013;1(1):14–7. <https://doi.org/10.12691/wjar-1-1-4>.
- Adzimah SK, Gbadam EK. Modification of the designs of cassava grating and cassava dough pressing machines into a single automated unit. *Eur J Sci Res* 2009; 38:306–14.
- Kolawole OP, Agbetoye LAS. Engineering research to improve cassava processing technology. *Int J Food Eng* 2007;3(6). <https://doi.org/10.2202/1556-3758.1311>.
- Ibrahim G, Wa A. Design and fabrication of cassava processing machine: the necessary aid for technological renaissance. *Iconic Res Eng J* 2022;5:321–33.
- Sadiku MN, Chukwu UC, Sadiku JO. Traditional African Food: An Introduction. *Sch: J Nat Med Educ* 2023;2(3):99–109. (https://univerpubl.com/index.php/sch_olastic/article/view/794).
- Mischler S. Triboelectrochemical techniques and interpretation methods in tribocorrosion: a comparative evaluation. *Tribology Int* 2008;41(7):573–83. <https://doi.org/10.1016/j.triboint.2007.11.003>.
- Jellesen MS, Rasmussen AA, Hilbert LR. A review of metal release in the food industry. *Mater Corros* 2006;57(5):387–93. <https://doi.org/10.1002/maco.200503953>.
- Atapour M, Wei Z, Chaudhary H, Lendel C, Odnevall Wallinder I, Hedberg Y. Metal release from stainless steel 316L in whey protein - And simulated milk solutions under static and stirring conditions. *Food Control* 2019;101:163–72. <https://doi.org/10.1016/j.foodcont.2019.02.031>.
- Oskarsson, A., Alexander, J., 2022. Chapter 7 - Toxic metals in food. In G.F. Nordberg, M. Costa (Eds.), *Handbook on the Toxicology of Metals (Fifth Edition)* (pp. 183–207). Academic Press, <https://doi.org/10.1016/B978-0-12-823292-7.00005-X>.
- Mazinanian N, Herting G, Odnevall I, Hedberg Y. Metal release and corrosion resistance of different stainless steel grades in simulated food contact. *Corros -Houst Tx* 2016;72:775–90. <https://doi.org/10.5006/2057>.
- EVM, 2002. Expert Group on Vitamins and Minerals, Review of Chromium (www.food.gov.uk/multimedia/pdfs/reviewofchrom.pdf).
- Keitel, S. Metals and alloys used in food contact materials and articles, a practical guide for manufacturers and regulators. In ISBN: 978–92-871–7703-2, Council of Europe: Strasbourg, France, 2013.
- EFSA, 2006. Tolerable upper intake levels for vitamins and minerals., in: European Food Safety Authority, Scientific Committee on Food, Scientific Panel on Dietetic Products, Nutrition and Allergies. (https://www.efsa.europa.eu/sites/default/files/efsa_rep/blobserver_assets/ndatolerableuil.pdf).
- Kuligowski J, Halperin KM. Stainless steel cookware as a significant source of nickel, chromium, and iron. *Arch Environ Contam Toxicol* 1992;23(2):211–5. <https://doi.org/10.1007/bf00212277>.
- Coles C, Crawford J, Roney N, Todd GD, Williams M. Draft Toxicological profile for manganese. *Cent Dis Control Prev* 2008. (https://stacks.cdc.gov/view/cdc/5167/cdc_5167_DS1.pdf).
- Anses, 2011. Second French Total Diet Study (TDS 2). (<https://www.anses.fr/en/system/files/PASER2006sa0361Ra1EN.pdf>).
- National Food Agency (1997). Danish Food Monitoring Programme: 1996 review: based on the report Food monitoring 1988–1992.
- Veien, N.K. (1989). Nickel dermatitis: Its relationship to food and experimental oral challenge. In: Nickel and the Skin: Immunology and Toxicology (Maibach, H. I., Menné, T., editors), pp. 165–178. CRC Press, Inc. Boca Raton, Florida.
- Veien NK, Menné T. Nickel contact allergy and a nickel-restricted diet. *Seminars in Dermatology* 1990;9(3):197–205.

- [27] WHO, 2011. Guidelines for drinking-water quality, Fourth ed. (<https://www.who.int/publications-detail-redirect/9789241549950>).
- [28] Fischer-Cripps AC. The Hertzian contact surface. *J Mater Sci* 1999;34(1):129–37. <https://doi.org/10.1023/A:1004490230078>.
- [29] Zhu, X., 2012. Tutorial on hertz contact stress, (https://kratosmultiphysics.github.io/Examples/contact_structural_mechanics/validation/hertz_full/data/OPT I-521-Tutorial-on-Hertz-contact-stress-Xiaoyin-Zhu.pdf).
- [30] Pius P, Nwigbo S. Design, fabrication, static and dynamic simulation of a cassava peeling machine. *Int J Recent Trends Eng Res* 2017;3(11):283–8.
- [31] Seth O. A review on the performance of some cassava peeling machines developed. *North Am Acad Res J* 2020;3(2):97–162. <https://doi.org/10.5281/zenodo.3669373>.
- [32] Alli OD, Abolarin MS. Design modification of a cassava attrition peeling machine. *J Phys: Conf Ser* 2019;1378:032029. <https://doi.org/10.1088/1742-6596/1378/3/032029>.
- [33] Eddy PP, Chuka NS, Omeiza OE, Chukwuemeka OH, Peter CO, Andrew AO. Dynamic analysis of fatigue life prediction on the shafts of a modern cassava peeling machine for safe and economic use. *J Eng Res Rep* 2021;20:117–30. <https://doi.org/10.9734/JERR/2021/v20i417301>.
- [34] Longhitano GA, García IM, Arenas MA, de Damborenea JJ, Maciel Filho R, Conde A. Effect of designed pore size on electrochemical, wear, and tribocorrosion behavior of additively manufactured Ti-6Al-4V lattice structures. *Addit Manuf* 2024;79:103931. <https://doi.org/10.1016/j.addma.2023.103931>.
- [35] Biesinger MC. Accessing the robustness of adventitious carbon for charge referencing (correction) purposes in XPS analysis: Insights from a multi-user facility data review. *Appl Surf Sci* 2022;597:153681. <https://doi.org/10.1016/j.apsusc.2022.153681>.
- [36] Biesinger M, Brown K, Mycroft JR, Davidson RD, McIntyre N. X-ray photoelectron spectroscopy studies of chromium compounds. *Surf Interface Anal* 2004;36:1550–63. <https://doi.org/10.1002/sia.1983>.
- [37] Biesinger M, Payne B, Grosvenor A, Lau L, Gerson A, Smart R. Resolving surface chemical states in XPS analysis of first row transition metals, oxides and hydroxides: Cr, Mn, Fe, Co and Ni. *Appl Surf Sci* 2011;257:2717–30. <https://doi.org/10.1016/j.apsusc.2010.10.051>.
- [38] Mazinanian N, Hedberg Y. Metal release mechanisms for passive stainless steel in citric acid at weakly acidic pH. *J Electrochem Soc* 2016;163:C686–93. <https://doi.org/10.1149/2.1041610jes>.
- [39] Gates JD. Two-body and three-body abrasion: a critical discussion. *Wear* 1998;214(1):139–46. [https://doi.org/10.1016/S0043-1648\(97\)00188-9](https://doi.org/10.1016/S0043-1648(97)00188-9).
- [40] Kirk B, Wilson AS, Stachowiak G. The morphology and composition of the superficial zone of mammalian articular cartilage. *J Orthop Rheumatol* 1993;6(1):21–8.
- [41] Sun Y, Rana V. Tribocorrosion behaviour of AISI 304 stainless steel in 0.5M NaCl solution. *Mater Chem Phys* 2011;129(1):138–47. <https://doi.org/10.1016/j.matchemphys.2011.03.063>.
- [42] Ben Saada F, Ben Saada M, Elleuch K, Ponthiaux P. Nanocrystallized surface effect on the tribocorrosion behavior of AISI 420. *Lubricants* 2022;10:304. <https://doi.org/10.3390/lubricants10110304>.
- [43] Matin S, Toorandaz S, Nikpour S, Abdolvand H, Toyserkani E, Hedberg YS. A bio-tribocorrosion comparison between additively manufactured and forged Ti6Al4V parts. *Addit Manuf Lett* 2023;7:100156. <https://doi.org/10.1016/j.addlet.2023.100156>.
- [44] Kolman DG, Ford DK, Butt DP, Nelson TO. Corrosion of 304 stainless steel exposed to nitric acid-chloride environments. *Corros Sci* 1997;39(12):2067–93. [https://doi.org/10.1016/S0010-938X\(97\)00092-9](https://doi.org/10.1016/S0010-938X(97)00092-9).
- [45] Zhang X, Zagidulin D, Shoesmith D. Characterization of film properties on the NiCrMo Alloy C-2000. *Electrochim Acta* 2013;89:814–22. <https://doi.org/10.1016/j.electacta.2012.11.029>.
- [46] Hedberg Y, Norell M, Linhardt P, Bergqvist H, Odnevall I. Influence of surface oxide characteristics and speciation on corrosion, electrochemical properties and metal release of atomized 316L stainless steel powders. *Int J Electrochem Sci* 2012;7:11655–77. [https://doi.org/10.1016/S1452-3981\(23\)16495-9](https://doi.org/10.1016/S1452-3981(23)16495-9).
- [47] Olefjord I, Wegrelius L. Surface analysis of passive state. *Corros Sci* 1990;31:89–98. [https://doi.org/10.1016/0010-938X\(90\)90095-M](https://doi.org/10.1016/0010-938X(90)90095-M).
- [48] Lv J, Guo W, Liang T, Yang M. The effects of ball milling time and surface enriched chromium on microstructures and corrosion resistance of AISI 304 stainless steel. *Mater Chem Phys* 2017;197:79–86. <https://doi.org/10.1016/j.matchemphys.2017.05.026>.
- [49] Hedberg Y, Wang X, Hedberg J, Lundin M, Blomberg E, Odnevall Wallinder I. Surface-protein interactions on different stainless steel grades: effects of protein adsorption, surface changes and metal release. *J Mater Sci: Mater Med* 2013;24(4):1015–33. <https://doi.org/10.1007/s10856-013-4859-8>.
- [50] Feng X, Wu T, Luo J-I, Lu X. Degradation of passive film on 304 stainless steel in a simulated concrete pore solution under alternating temperature condition. *Cem Concr Compos* 2020;112:103651. <https://doi.org/10.1016/j.cemconcomp.2020.103651>.
- [51] Oluwole OO, Atanda PO, Odekunbi OA, Odegbaju E. Corrosion behaviour of 18/8 stainless steel and nickel-plated low carbon steel in cassava fluid. *J Miner Mater Charact Eng* 2009;8:803–11. <https://doi.org/10.4236/jmmce.2009.810069>.
- [52] Varmaziar S, Atapour M, Hedberg YS. Corrosion and metal release characterization of stainless steel 316L weld zones in whey protein solution. *npj Mater Degrad* 2022;6(1):19. <https://doi.org/10.1038/s41529-022-00231-7>.
- [53] Hedberg YS. Role of proteins in the degradation of relatively inert alloys in the human body. *npj Mater Degrad* 2018;2(1):26. <https://doi.org/10.1038/s41529-018-0049-y>.
- [54] Kocijan A, Milošev I, Pihlar B. The influence of complexing agent and proteins on the corrosion of stainless steels and their metal components. *J Mater Sci Mater Med* 2003;14:69–77. <https://doi.org/10.1023/A:1021505621388>.
- [55] Hedberg Y, Midander K. Size matters: mechanism of metal release from 316L stainless steel particles is governed by size-dependent properties of the surface oxide. *Mater Lett* 2014;122:223–6. <https://doi.org/10.1016/j.matlet.2014.02.034>.
- [56] Schwertmann U. Solubility and dissolution of iron oxides. *Plant Soil* 1991;130(1):1–25. <https://doi.org/10.1007/BF00011851>.
- [57] Casaroli A, Boniardi M, Dalipi R, Borgese L, Depero LE. Procedure optimization of type 304 and 420B stainless steels release in acetic acid. *Food Control* 2020;120:107509. <https://doi.org/10.1016/j.foodcont.2020.107509>.
- [58] Herting G, Odnevall I, Leygraf C. Factors that influence the release of metals from stainless steels exposed to physiological media. *Corros Sci* 2006;48:2120–32. <https://doi.org/10.1016/j.corsci.2005.08.006>.
- [59] Herting G, Odnevall I, Leygraf C. A comparison of release rates of Cr, Ni, and Fe from STainless Steel Alloys and the Pure Metals Exposed to Simulated Rain Events. *J Electrochem Soc* 2005;152:B23–9. <https://doi.org/10.1149/1.1834901>.
- [60] Melo-Máximo L, Salas O, Melo-Máximo D, Oseguera J, López-Hirata VM, Torres RD, et al. Performance of Cr oxide coatings on 304 steel against metal dusting. *Surf Coat Technol* 2013;237:39–50. <https://doi.org/10.1016/j.surfcoat.2013.08.038>.
- [61] Ha H-Y, Lee T-H, Kim S-D, Jang J, Moon J. Improvement of the corrosion resistance by addition of Ni in lean duplex stainless steels. *Metals* 2020;10:891. <https://doi.org/10.3390/met10070891>.
- [62] Feyzi M, Fallahnezhad K, Taylor M, Hashemi R. What role do normal force and frequency play in the tribocorrosion behaviour of Ti-6Al-4 V alloy? *Tribology Int* 2022;172:107634. <https://doi.org/10.1016/j.triboint.2022.107634>.
- [63] Mali SA, Zhu D, Liu Y, Gilbert JL. Fretting crevice corrosion of 316 L stainless steel in physiological phosphate buffered saline: lead, potential and alloy counterface effects. *Tribology Int* 2021;164:107198. <https://doi.org/10.1016/j.triboint.2021.107198>.
- [64] Harry T, Taiwo A, Oduola K, Joel O. Performance evaluation of local cassava starches with imported starch for drilling fluid. *Am J Eng Res* 2016;5:111–20.
- [65] Street RA, Goessler W, Naidoo S, Shezi B, Cele N, Rieger J, et al. Exposure to lead and other toxic metals from informal foundries producing cookware from scrap metal. *Environ Res* 2020;191:109860. <https://doi.org/10.1016/j.envres.2020.109860>.
- [66] Habimaana S, Gumisiriza H, Birungi G. Trace metal leaching from cookware locally fabricated from scrap metal: a case study of Ntungamo District, Uganda. *Am J Anal Chem* 2022;13:314–30. <https://doi.org/10.4236/ajac.2022.139022>.
- [67] Weidenhamer JD, Fitzpatrick MP, Biro AM, Kobunski PA, Hudson MR, Corbin RW, et al. Metal exposures from aluminum cookware: an unrecognized public health risk in developing countries. *Sci Total Environ* 2017;579:805–13. <https://doi.org/10.1016/j.scitotenv.2016.11.023>.
- [68] Ali Sultan SA, Ahmed Khan F, Wahab A, Fatima B, Khalid H, Bahader A, et al. Assessing leaching of potentially hazardous elements from cookware during cooking: a serious public health concern. *Toxics* 2023;11(7):640. <https://doi.org/10.3390/toxics11070640>.

Supplementary information

Tribocorrosion and metal release from austenitic stainless steels 304 and 201 in simulated cassava food contact

R. Addai, T. Olowoyo, J. D. Henderson, T. E. Standish, U. Eduok, Y. S. Hedberg

Content: Figures S1-S25.

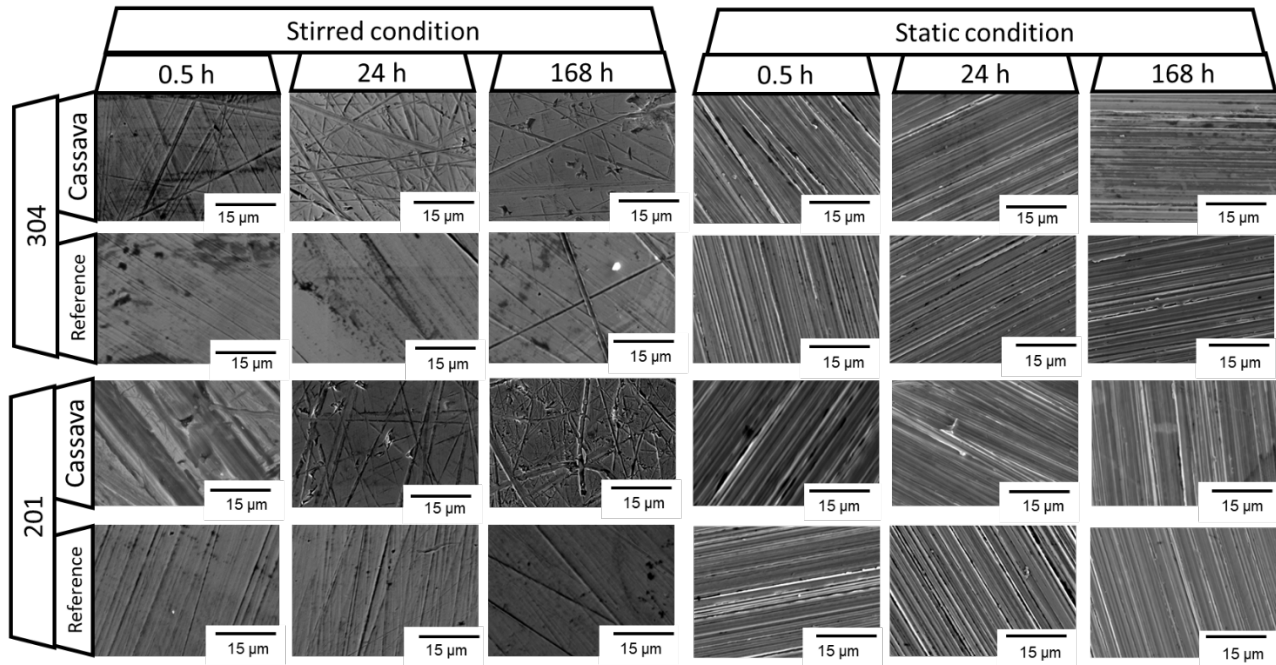


Figure S1. SEM images of representative stainless steel 201 and 304 coupons exposed under stirred and static conditions at room temperature for 0.5, 24, and 168 h in the cassava slurry and reference solution.

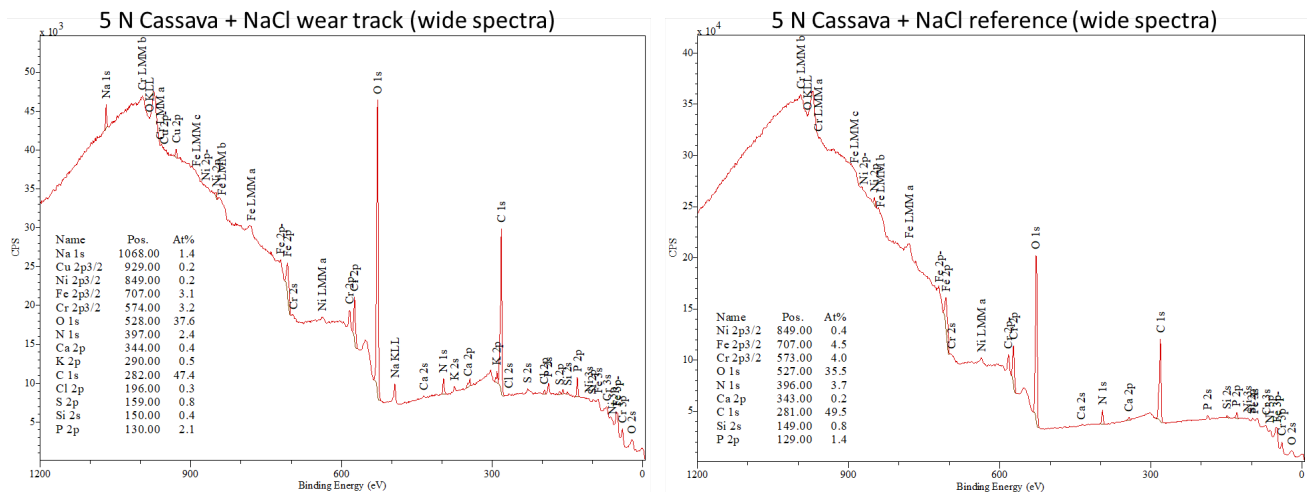


Figure S2. Wide spectra (XPS) of stainless steel 304 after tribocorrosion exposure under 5 N load to cassava + NaCl solution at room temperature. Two different spots are shown: inside the wear track (left) and outside of the wear track (right).

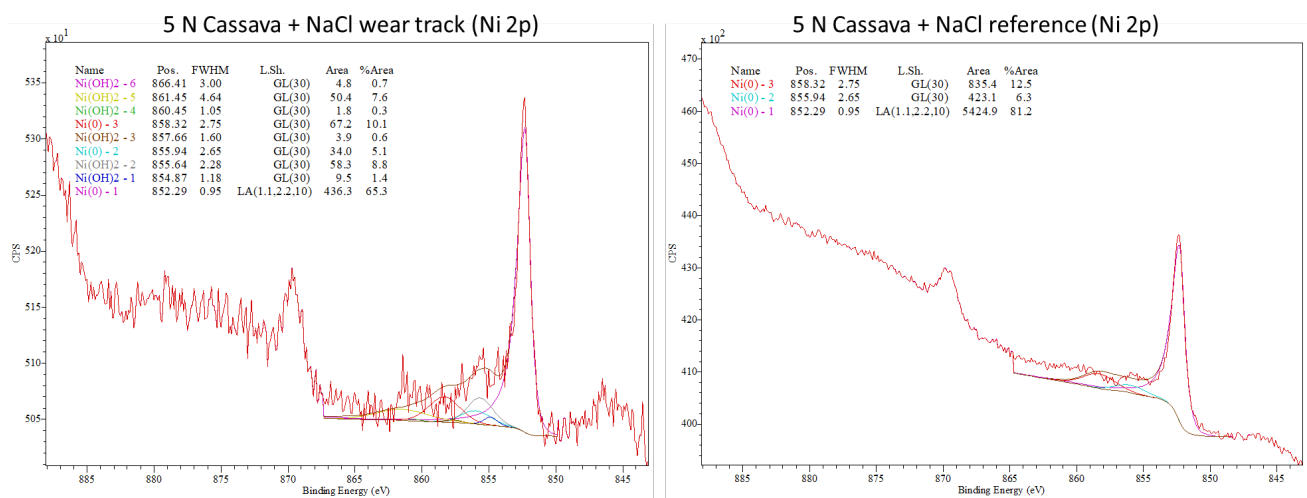


Figure S3. High-resolution Ni 2p spectra (XPS) of stainless steel 304 after tribocorrosion exposure under 5 N load to cassava + NaCl solution at room temperature. Two different spots are shown: inside the wear track (left) and outside of the wear track (right).

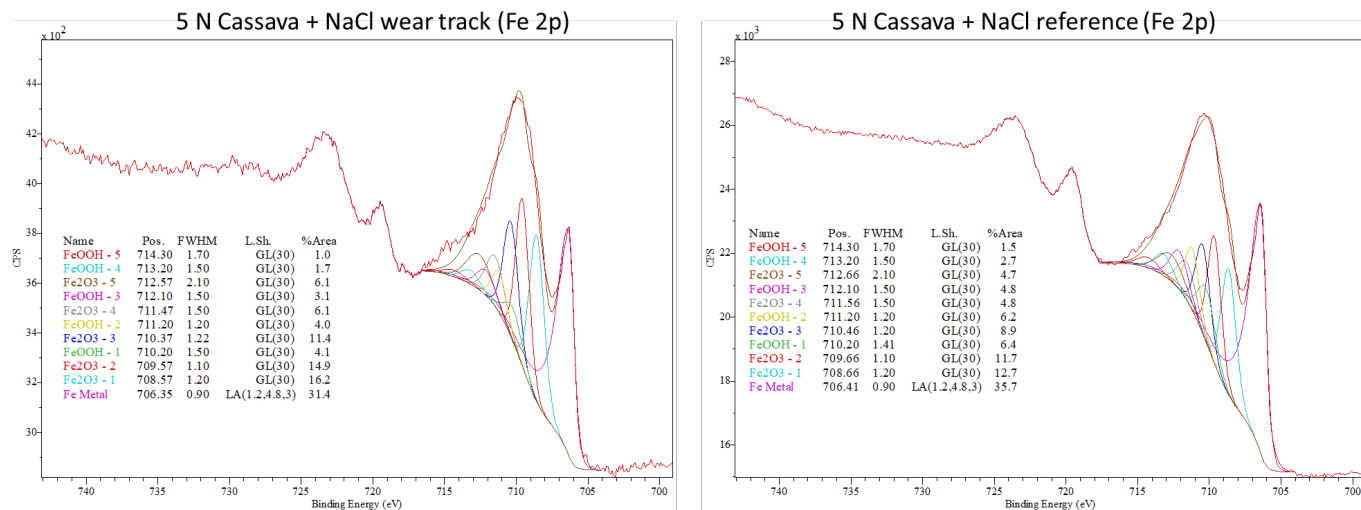


Figure S4. High-resolution Fe 2p spectra (XPS) of stainless steel 304 after tribocorrosion exposure under 5 N load to cassava + NaCl solution at room temperature. Two different spots are shown: inside the wear track (left) and outside of the wear track (right).

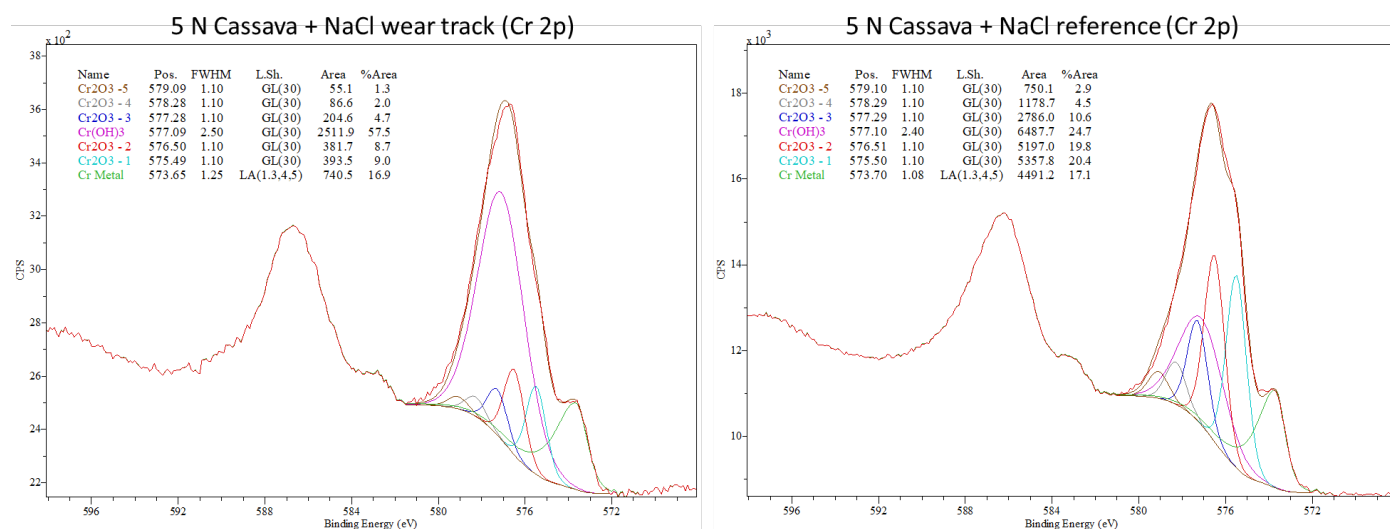


Figure S5. High-resolution Cr 2p spectra (XPS) of stainless steel 304 after tribocorrosion exposure under 5 N load to cassava + NaCl solution at room temperature. Two different spots are shown: inside the wear track (left) and outside of the wear track (right).

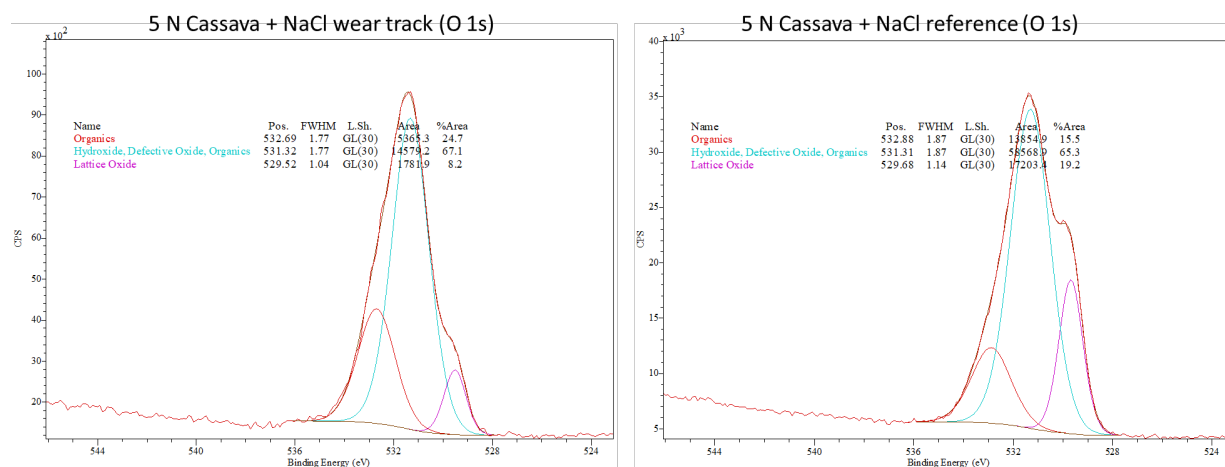


Figure S6. High-resolution O 1s spectra (XPS) of stainless steel 304 after tribocorrosion exposure under 5 N load to cassava + NaCl solution at room temperature. Two different spots are shown: inside the wear track (left) and outside of the wear track (right).

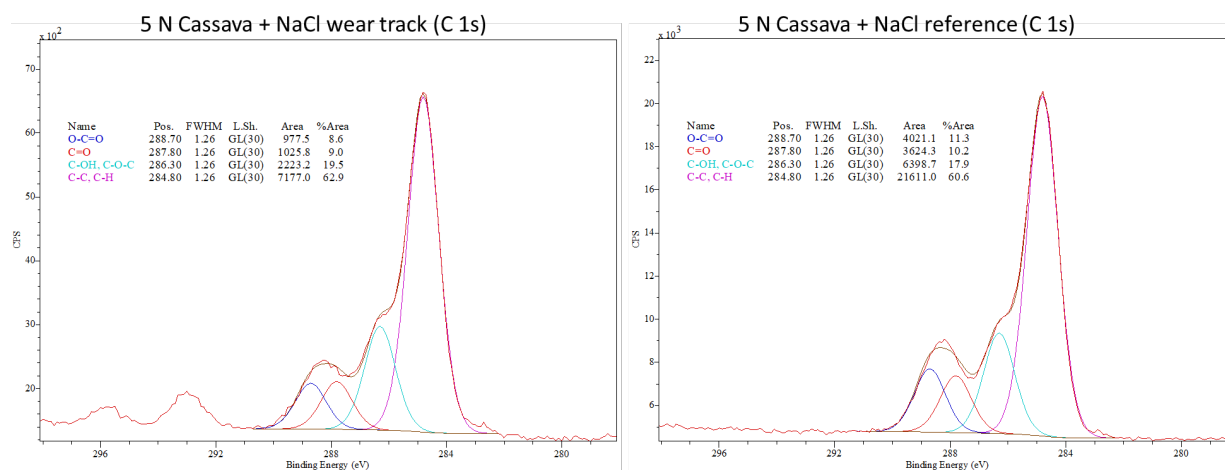


Figure S7. High-resolution C 1s spectra (XPS) of stainless steel 304 after tribocorrosion exposure under 5 N load to cassava + NaCl solution at room temperature. Two different spots are shown: inside the wear track (left) and outside of the wear track (right).

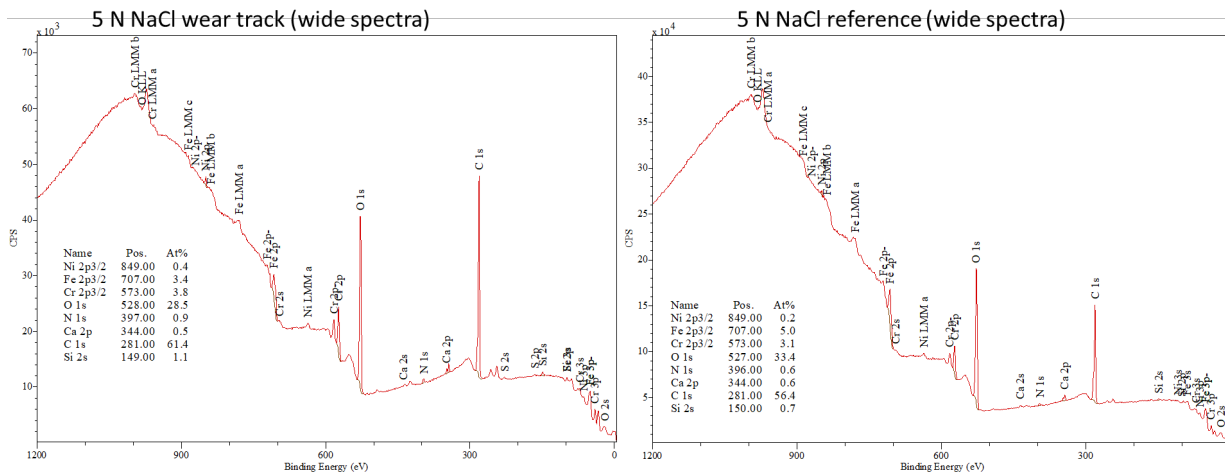


Figure S8. Wide spectra (XPS) of stainless steel 304 after tribocorrosion exposure under 5 N load to reference (no cassava) NaCl solution at room temperature. Two different spots are shown: inside the wear track (left) and outside of the wear track (right).

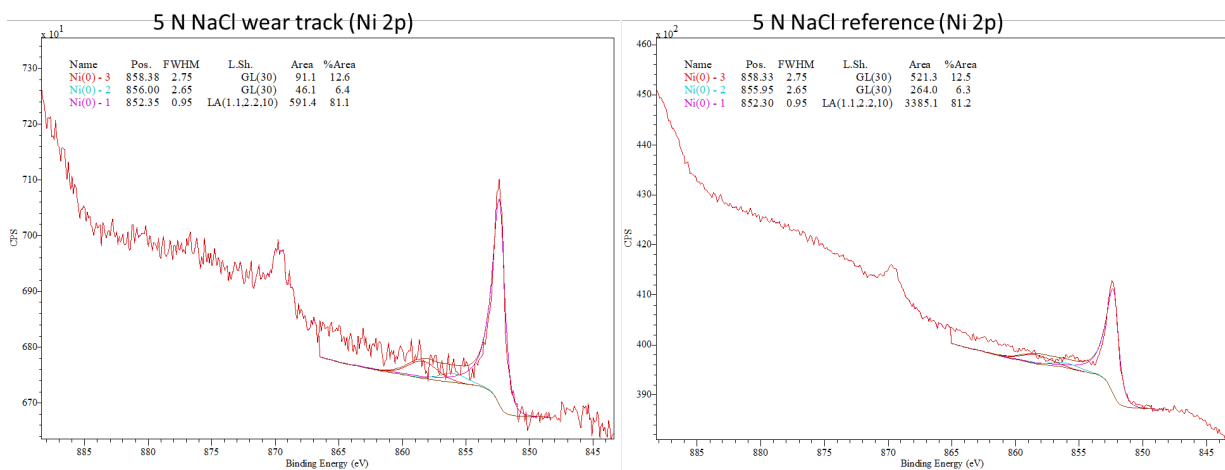


Figure S9. High-resolution Ni 2p spectra (XPS) of stainless steel 304 after tribocorrosion exposure under 5 N load to reference (no cassava) NaCl solution at room temperature. Two different spots are shown: inside the wear track (left) and outside of the wear track (right).

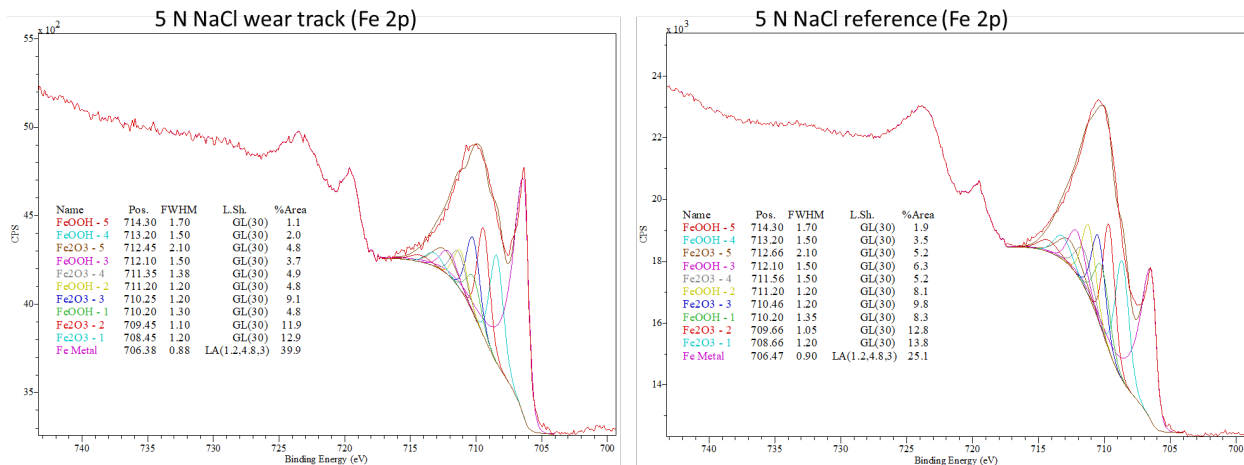


Figure S10. High-resolution Fe 2p spectra (XPS) of stainless steel 304 after tribocorrosion exposure under 5 N load to reference (no cassava) NaCl solution at room temperature. Two different spots are shown: inside the wear track (left) and outside of the wear track (right).

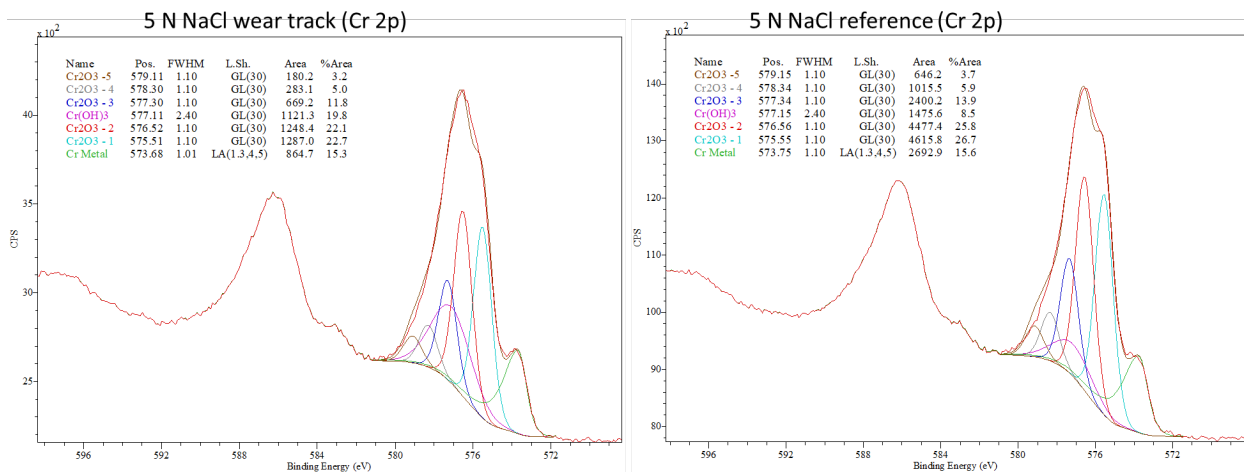


Figure S11. High-resolution Cr 2p spectra (XPS) of stainless steel 304 after tribocorrosion exposure under 5 N load to reference (no cassava) NaCl solution at room temperature. Two different spots are shown: inside the wear track (left) and outside of the wear track (right).

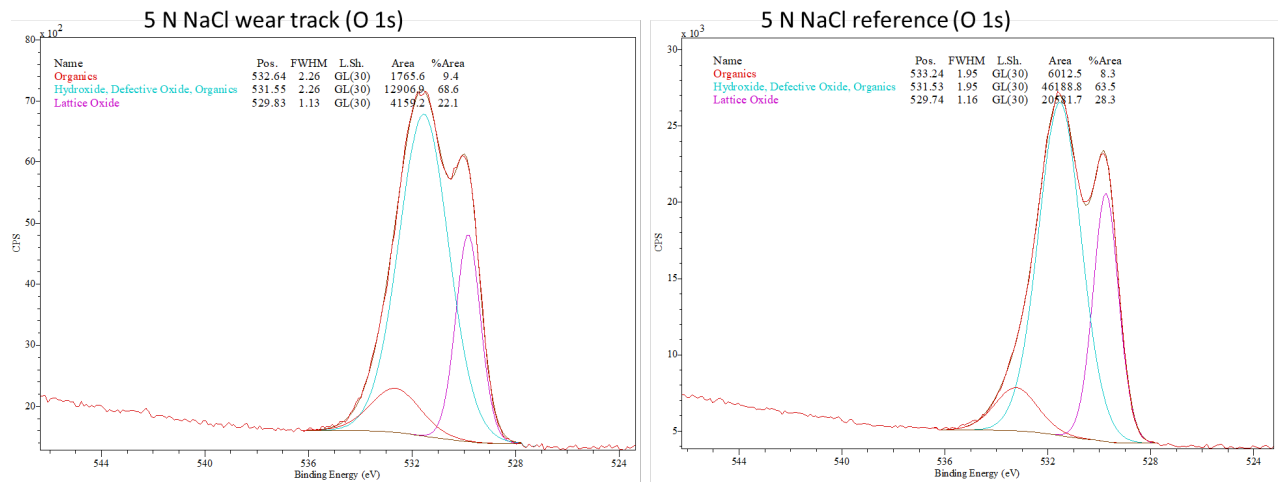


Figure S12. High-resolution O 1s spectra (XPS) of stainless steel 304 after tribocorrosion exposure under 5 N load to reference (no cassava) NaCl solution at room temperature. Two different spots are shown: inside the wear track (left) and outside of the wear track (right).

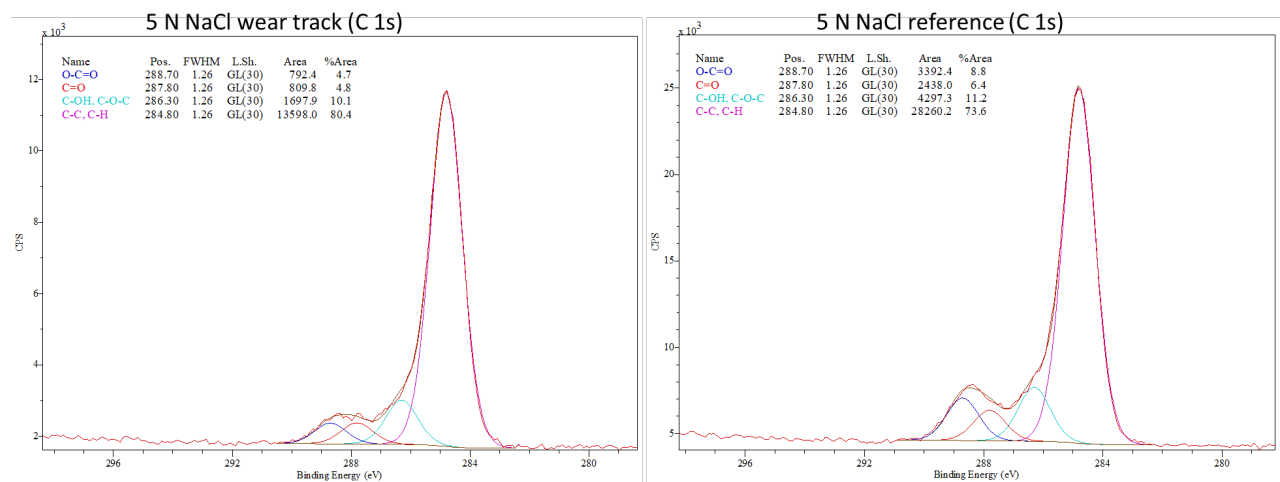


Figure S13. High-resolution C 1s spectra (XPS) of stainless steel 304 after tribocorrosion exposure under 5 N load to reference (no cassava) NaCl solution at room temperature. Two different spots are shown: inside the wear track (left) and outside of the wear track (right).

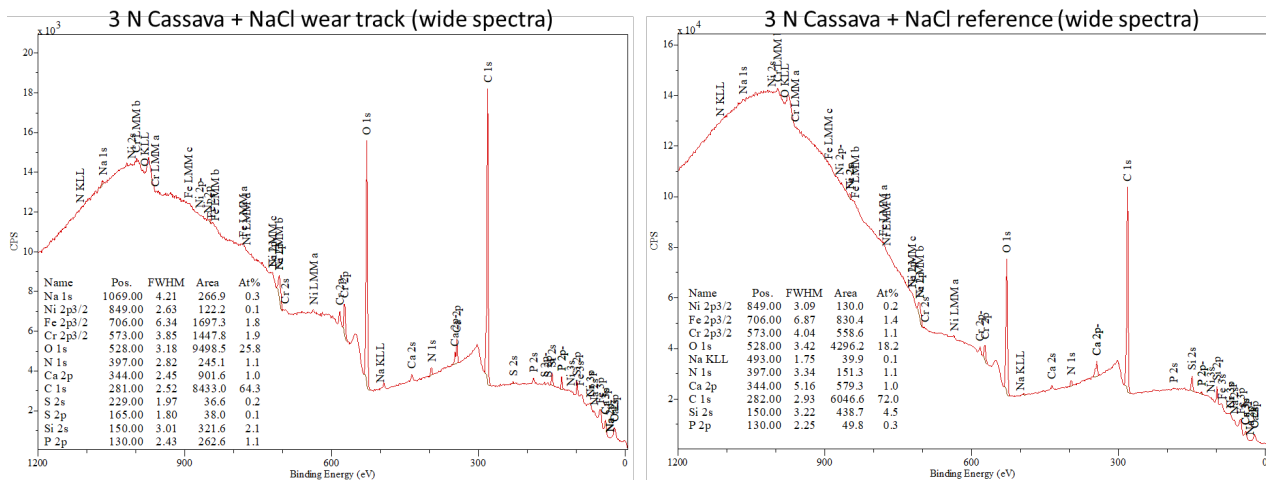


Figure S14. Wide spectra (XPS) of stainless steel 304 after tribocorrosion exposure under 3 N load to cassava + NaCl solution at room temperature. Two different spots are shown: inside the wear track (left) and outside of the wear track (right).

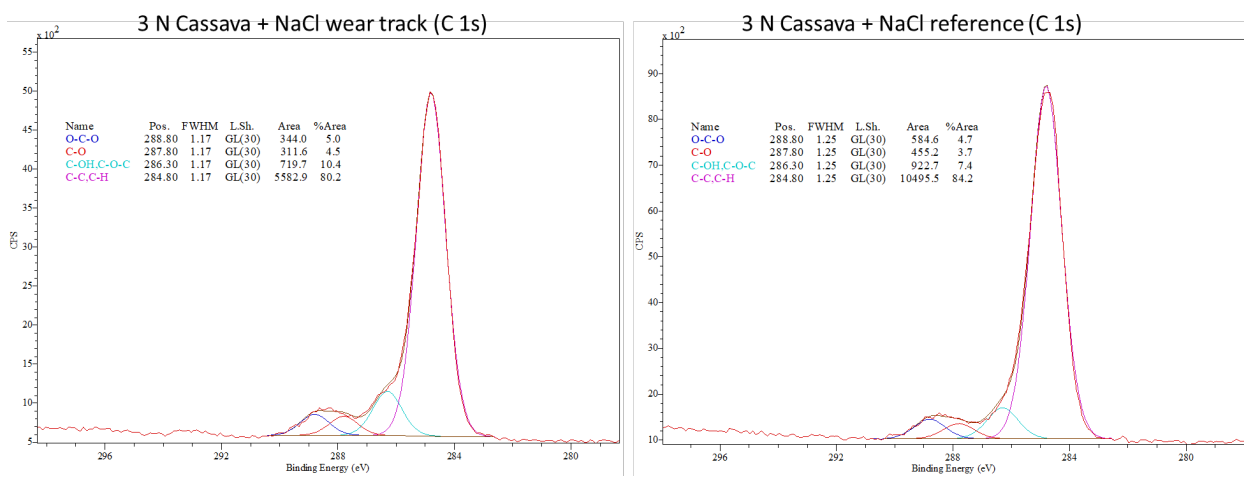


Figure S15. High-resolution C 1s spectra (XPS) of stainless steel 304 after tribocorrosion exposure under 3 N load to cassava + NaCl solution at room temperature. Two different spots are shown: inside the wear track (left) and outside of the wear track (right).

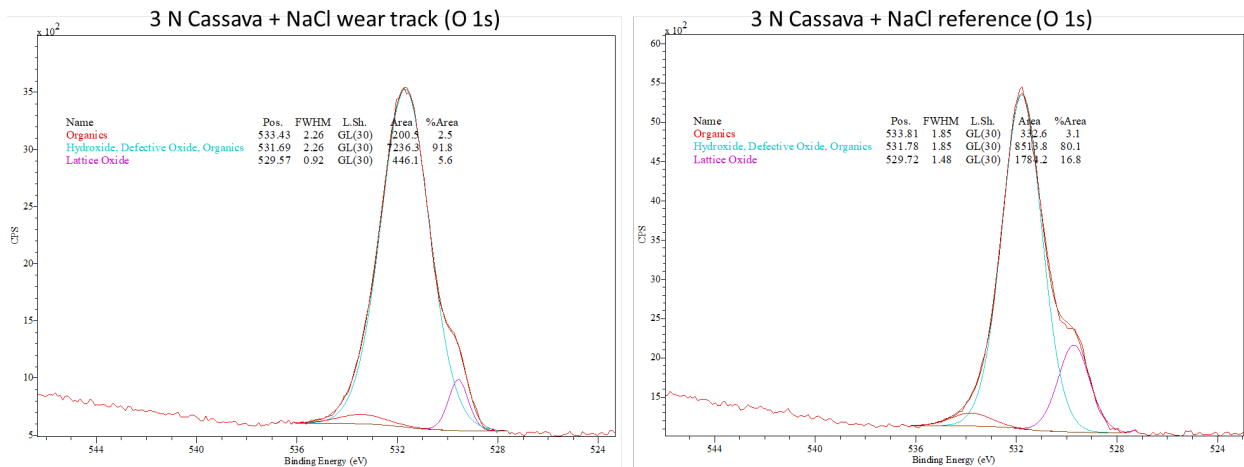


Figure S16. High-resolution O 1s spectra (XPS) of stainless steel 304 after tribocorrosion exposure under 3 N load to cassava + NaCl solution at room temperature. Two different spots are shown: inside the wear track (left) and outside of the wear track (right).

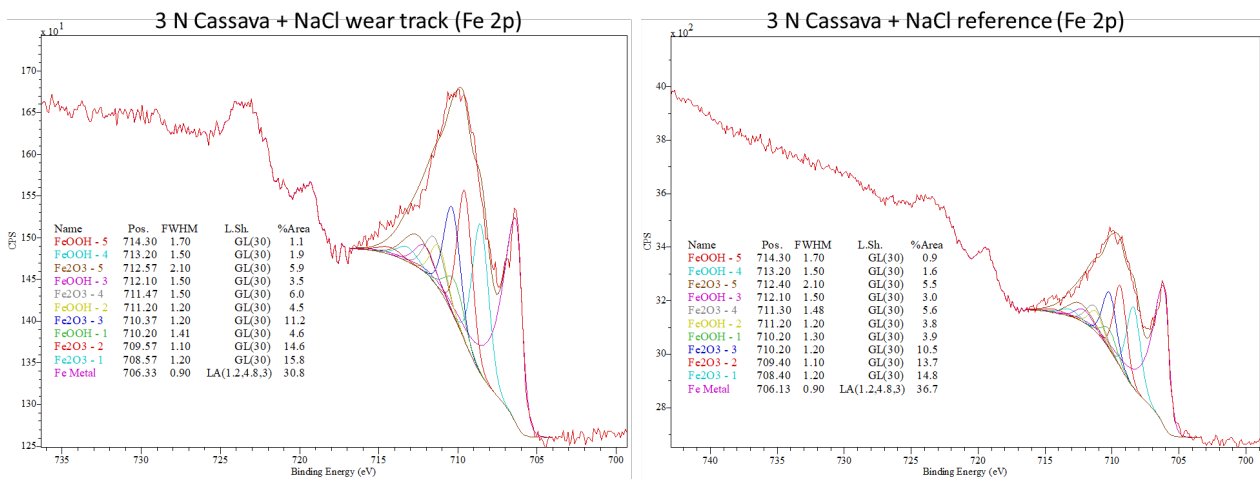


Figure S17. High-resolution Fe 2p spectra (XPS) of stainless steel 304 after tribocorrosion exposure under 3 N load to cassava + NaCl solution at room temperature. Two different spots are shown: inside the wear track (left) and outside of the wear track (right).

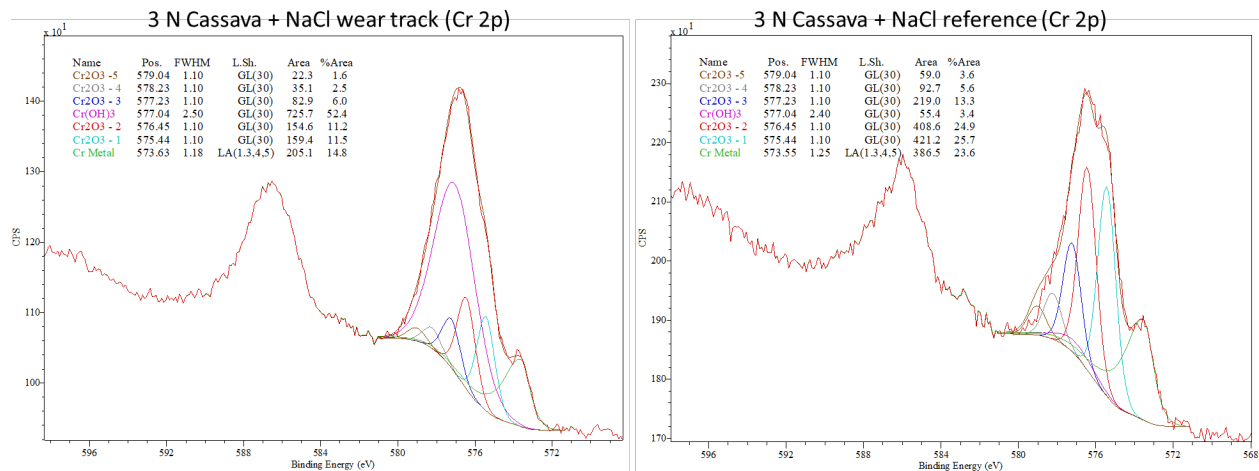


Figure S18. High-resolution Cr 2p spectra (XPS) of stainless steel 304 after tribocorrosion exposure under 3 N load to cassava + NaCl solution at room temperature. Two different spots are shown: inside the wear track (left) and outside of the wear track (right).

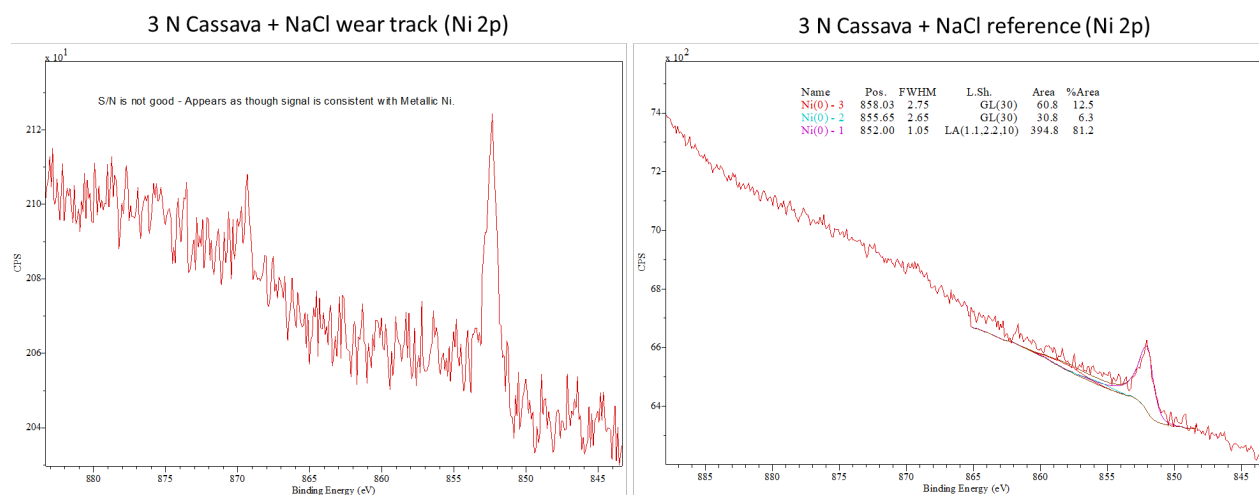


Figure S19. High-resolution Ni 2p spectra (XPS) of stainless steel 304 after tribocorrosion exposure under 3 N load to cassava + NaCl solution at room temperature. Two different spots are shown: inside the wear track (left) and outside of the wear track (right).

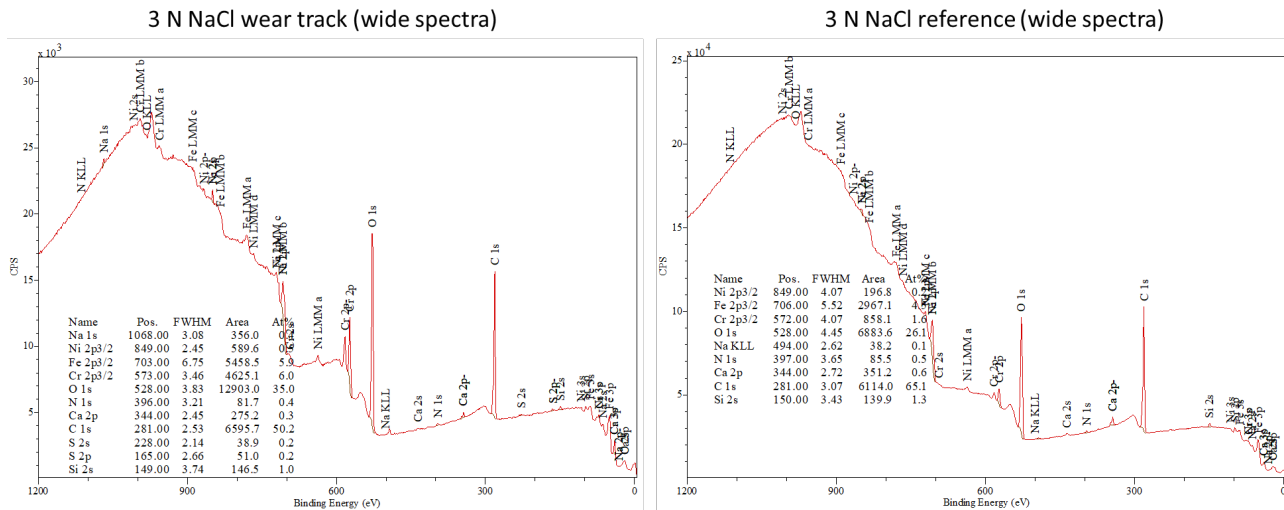


Figure S20. Wide spectra (XPS) of stainless steel 304 after tribocorrosion exposure under 3 N load to reference NaCl (no cassava) solution at room temperature. Two different spots are shown: inside the wear track (left) and outside of the wear track (right).

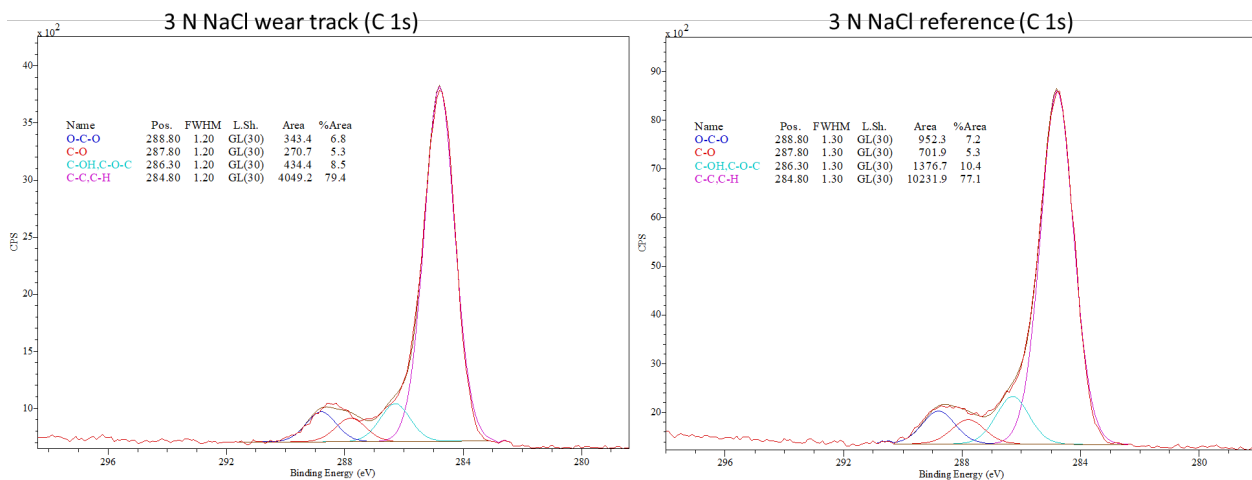


Figure S21. High-resolution C 1s spectra (XPS) of stainless steel 304 after tribocorrosion exposure under 3 N load to reference NaCl (no cassava) solution at room temperature. Two different spots are shown: inside the wear track (left) and outside of the wear track (right).

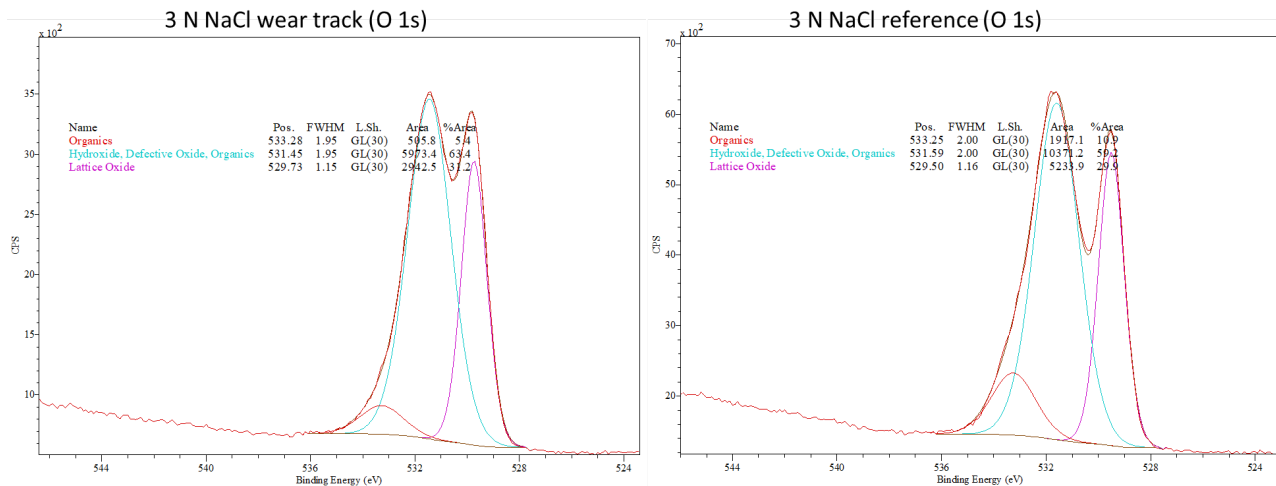


Figure S22. High-resolution O 1s spectra (XPS) of stainless steel 304 after tribocorrosion exposure under 3 N load to reference NaCl (no cassava) solution at room temperature. Two different spots are shown: inside the wear track (left) and outside of the wear track (right).

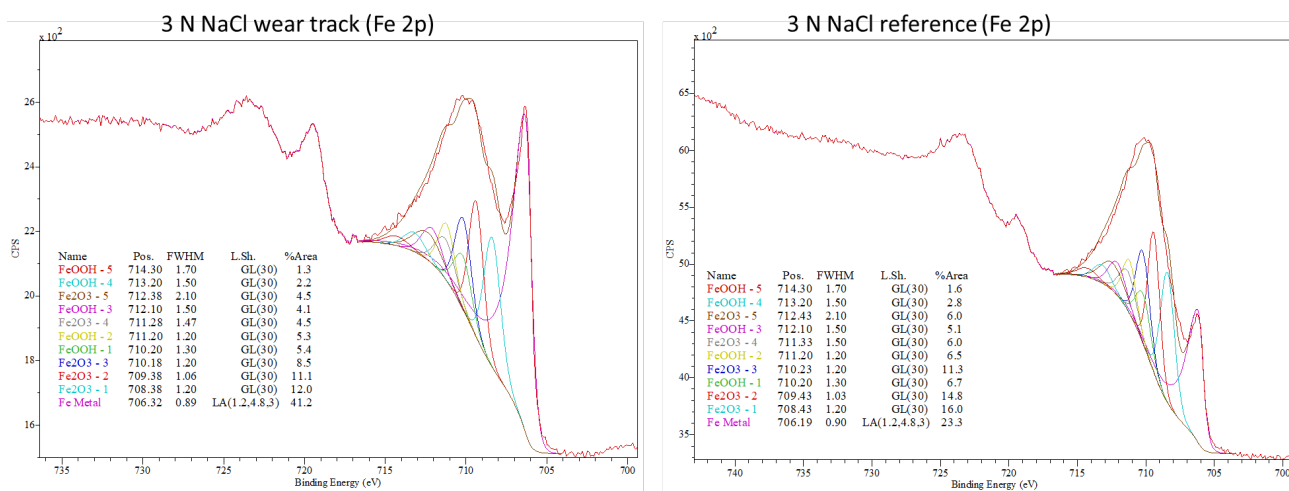


Figure S23. High-resolution Fe 2p spectra (XPS) of stainless steel 304 after tribocorrosion exposure under 3 N load to reference NaCl (no cassava) solution at room temperature. Two different spots are shown: inside the wear track (left) and outside of the wear track (right).

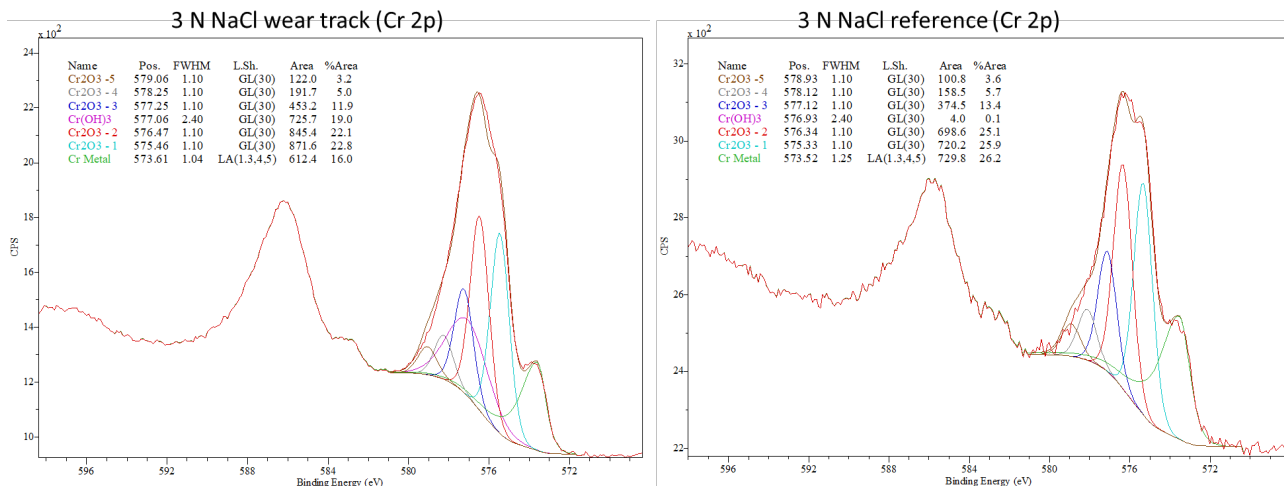


Figure S24. High-resolution Cr 2p spectra (XPS) of stainless steel 304 after tribocorrosion exposure under 3 N load to reference NaCl (no cassava) solution at room temperature. Two different spots are shown: inside the wear track (left) and outside of the wear track (right).

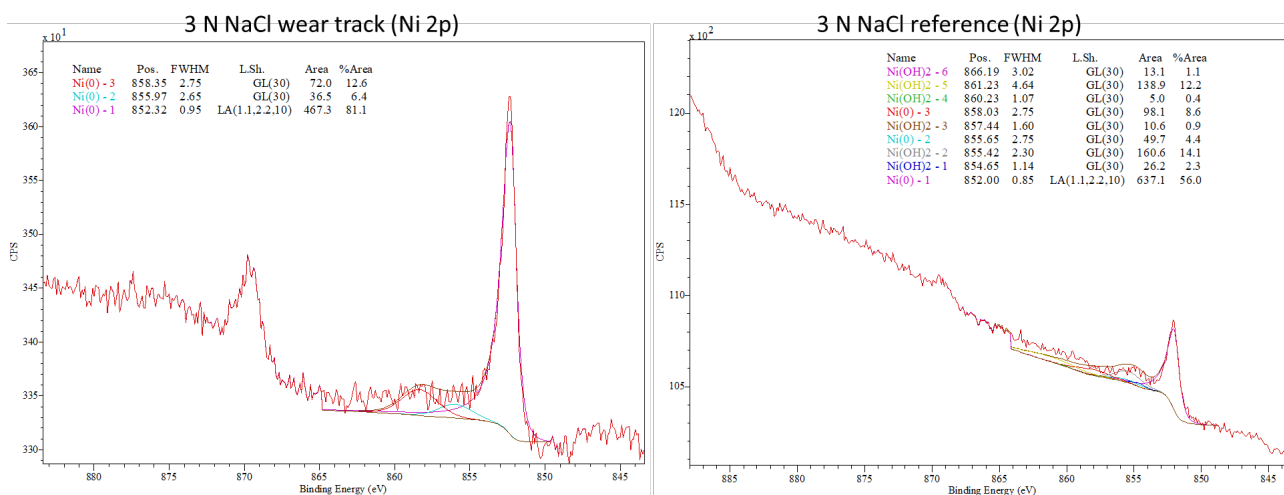


Figure S25. High-resolution Ni 2p spectra (XPS) of stainless steel 304 after tribocorrosion exposure under 3 N load to reference NaCl (no cassava) solution at room temperature. Two different spots are shown: inside the wear track (left) and outside of the wear track (right).